INVESTIGATING THE EFFECT OF CLAY MINERALS ON A SANDSTONE RESERVOIR: A ROCK PHYSICS ANALYSIS OF MAGNOLIA FIELD GULF OF MEXICO

A Thesis Presented to

the Faculty of the Department of Earth and Atmospheric Sciences

University of Houston

---

in Partial fulfilment

of the Requirements for the Degree

Master of Science

By

John Ireyemi Adesoji

December 2014

INVESTIGATING THE EFFECT OF CLAY MINERALS ON A SANDSTONE RESERVOIR: A ROCK PHYSICS ANALYSIS OF MAGNOLIA FIELD GULF OF MEXICO

John Ireyemi Adesoji

APPROVED:

Dr. Michael Murphy, Chairman

Dr. De-Hau Han, Co-Chairman

Dr. Evgeny Chesnokov, Member

Dr. Mosab Nasser, Member

Dean, College of Natural Sciences and Mathematics

ACKNOWLEDGEMENTS

My profound gratitude goes first to my Parakletos and various destiny coaches. I wish to appreciate all my committee members; Dr. Michael Murphy (Chairman), Dr. De-hua Han (Co-chairman), Dr. Chesnokov, Evgeny (Member) and Dr. Mosab Nasser (Member) for various constructive instructions and assistance at various points of the research.

I would especially like to acknowledge the geophysics professors and the staff of the Earth and Atmospheric Sciences Department for their commitment to excellence all through my program.

I really appreciate all the members of my family: my parents, Pastor T.A and Mrs. O.A. Adesoji, whom I dedicate this thesis to, and my siblings, Opeyemi (Late), Ayoyemi, Adeyemi, Olayemi and Oluwayemisi for their financial and moral support during the period of my study at the University of Houston. I am very grateful for the help rendered by Adeniyi Oluwasegun, Adepehin Ekundayo, Adeyemo Paul, Ahiabu Ivy, Akinleyimu Blessing, Babalola Ayodeji, Bankole Olabode, Dr. Arnold Oyem, Hui Li, Omoboya Bode, Oyetunji Oyedoyin, Oyepeju Alli, Xia Keyao and contributions of other colleagues during the period of this research; may the Big God bless you all.

.

INVESTIGATING THE EFFECT OF CLAY MINERALS ON A SANDSTONE RESERVOIR: A ROCK PHYSICS ANALYSIS OF MAGNOLIA FIELD GULF OF MEXICO

An Abstract of a Thesis

Presented to

the Faculty of the Department of Earth and Atmospheric Sciences

University of Houston

In Partial Fulfilment

of the Requirements for the Degree

Master of Science

By

John Ireyemi Adesoji

December 2014

ABSTRACT

Petrophysical and Rock physics approaches have been used to investigate the effects of clay minerals within delineated reservoirs from the Magnolia field, offshore Louisiana. It is generally known that reservoir sandstones are rarely deposited alone rather they occur alongside finer clay minerals which are often of varying mineralogy, morphology, and distribution. Clay minerals are members of the hydrous aluminous phyllosilicates that dominate the fined-grained fractions of reservoir rocks (Worthington, 2003).

A well-known approach often used to unravel clay mineral distributions within a clastic reservoir is through special core analysis. This process is capital intensive and usually gives non-continuous down-hole measurement. This study employs rock physics models to understand clay distribution within Magnolia field in the deep-water Northern Gulf of Mexico.

The Thomas–Stieber model is used to predict and describe the porosity-shale volume relations resulting from various mode of sandstone–shale mixing. The Dvorkin and Gutierrez model predicts the associated P-wave velocities. The combination of Thomas-Stieber and Dvorkin-Gutierrez models gives a higher degree of confidence while evaluating formation properties. From the above approach, dominant clay distribution pattern observed in the reservoirs delineated in Magnolia field are laminated clay. Dispersed and structural clays are rarely observed within the reservoirs. Findings from this research show that rock physics analysis can be used as an alternative to core analysis in determining clay distribution patterns and local reservoir studies.

TABLE OF CONTENTS

List of Figures

List of Tables

CHAPTER 1

INTRODUCTION

1.1 Background and Motivation

Over the years, the Gulf of Mexico has become a region of interest to geoscientists and reservoir engineers. As one of the leading sources of petroleum in the United States, its discovery has provided exciting opportunities for deep-water exploration and production. Nevertheless, a major challenge associated with deep-water exploration is the presence of over-pressure in reservoirs. It has been proposed that overpressure arises when the rate of sedimentation exceeds the ability of the sediments to drain into the rapidly formed basin resulting in the disequilibrium of the sediment (Flemings *et al.* 2001).

The connection between the elastic properties of rocks – such as P-wave velocity, S-wave velocity, poisson's ratio, P-impedance and bulk modulus and the reservoir properties (porosity, permeability, water saturation and clay content) is described by rock physics. Rock-physics has also gained importance in well conditioning, reservoir evaluation, rock modelling, time-lapse analysis and other drilling solutions. The reservoirs within the Magnolia field in my area of study are composed of fined-grained sand-silt sized feldspathic quartzose sandstone and some quantities of clays and clay minerals.

Typically, reservoir sandstones are not deposited alone but occur with finer clay minerals which are often of varying mineralogy, morphology and distribution. Clay minerals are members of the hydrous aluminous phyllosilicates that dominate

the fined-grained fractions of reservoir rocks (Worthington, 2003). The presence of clays and clay minerals within a petroleum reservoir makes such reservoirs difficult to characterize due to its abnormal effect on measured (sonic velocity) and estimated (porosity) properties of the reservoir, and the relationship between them (Wyllie *et al.* 1956; Darling, 2005). This effect has been known to lead to significant underestimation or overestimation of reservoir properties.

Conventionally, clay-mineral distributions in sandstone reservoirs are determined through special core analysis using a representative portion of the core sample. A freshly broken surface of the sample is mounted on an aluminium stub with carbon paint, and is given a thin coating of gold. The sample is then imaged under the Scanning Electron Microscope (SEM) to decipher the nature of the pore system, the distribution of clay minerals and other cements associated with the primary pore system. Minerals are also analysed using Energy Dispersive X-ray (EDX) to determine the elemental composition of particular minerals in a particular sample area. Though special core analysis has been useful for the characterization of these minerals, the technique is expensive and often generates non-continuous down-hole measurement.

This study focuses on employing a petrophysical and rock-physics approach to investigate the effect of the distribution of clay mineral in the Magnolia field and identify a pore-pressure effect on the reservoirs in the deep offshore of the Gulf of Mexico. Consequently, a reasonable prediction of clay mineral distributions within the reservoir will give reliable estimates of the volume of producible hydrocarbons in its pore spaces, and reduce uncertainties and risks in heterogeneous sandstone-reservoir production.

1.2 Research Objective

This thesis integrates petrophysical and rock physics to study the effect of clay heterogeneity and pore pressure on reservoir properties as it applies to a sandstone reservoir. The following are the technical objectives to this study:

- Increase the understanding of rock properties and local reservoir heterogeneities using log data.
- Understand the relationship between rock physics and reservoir quality
- Apply rock physics to model different clay-distribution patterns and to assess its effect on both elastic properties and reservoir properties.
- Build a site-specific rock physics model using appropriate theories to establish Velocity- Porosity Trends of the study area.

1.3 Thesis Overview

The first part of this thesis describes a detailed petrophysical evaluation on well-logs to determine the porosity (ϕ), water saturation (Sw), and lithology (Vsh) or shale volume fraction. This was followed by analyzing the well-logs in order to identify the reservoir zones.

The second part describes rock-physics modelling using the Thomas-Stieber model and the Yin-Marion-Dvorkin-Gutierrez model. The Thomas-Stieber model predicts the porosity resulting from various mixtures of sand and mud and describes the porosity-shale relations in clastic sediments (i.e., volumetrics). The Yin-Marion-Dvorkin-Gutierrez model predicts the associated P-wave velocities which quantitatively estimate the elastic property associated with clay distribution.

The third part describes the method used to estimate elastic rock-frame properties by analyzing the lithology and fluid saturation using rock-physics analysis. Gassman's equation was used to determine rock frame properties in shaly-sandstone formation, define a site-specific sandstone-shale system, and extracting shale properties from the log data.

The final part summarizes the results and the implication of clay and clay mineral within an overall continuum of reservoir behavioural characteristics. The project work flow is summarized in figure 1.1.

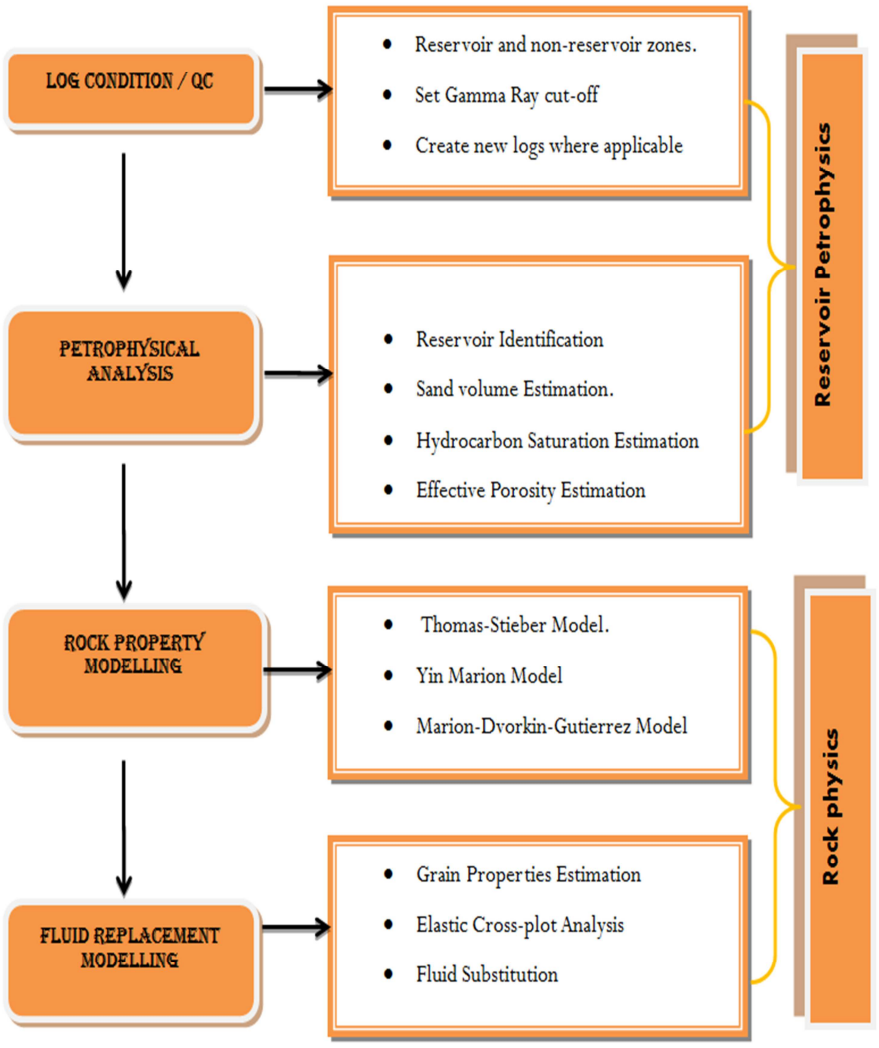

Figure 1.1: Project Workflow

1.4 Definitions

For clarity, it is necessary to first of all define terms that are used in petrophysics and the reservoir models that are used in conventional petrophysical evaluation, and how clay minerals are incorporated within them. In this study, the idea of clay minerals is the one occurring with sandstone reservoir rather than one of the intrinsic properties of a (pure) clay-mineral assemblage.

The following terms are used within the scope of petrophysics:

- Clay mineral: - A member of the hydrous aluminous phyllosilicates that dominate the fine fractions of reservoir rocks. The term 'clay mineral' refers to composition, not grain size (Worthington, 2003).
- Clay: - It is strictly a grain-size term with particle size diameter less than 3.9 μm (Worthington, 2003).
- Silt: - A grain-size term with particle size diameter between 3.9 and 62.5 μm.
- Bound water: - Electrochemically bound molecular water that is adsorbed at mineral surfaces as the result of an anion surface charge, which attracts free cations into an electrical double layer. This effect is most noticeable in the presence of clay minerals, for which it also includes interlayer molecular water.
- Shale: - An assemblage of silt, clay and clay minerals. Petrophysicists often assumes that shale comprises only clay minerals but in reality shale may contain more than 70% by volume of silt and larger detritus. Perfect shale is one that comprises 100% clay minerals, regardless of grain size, with no electrochemically free water. An imperfect shale comprises a significant

percentage of minerals other than clay minerals. It contains both free and bound waters (Worthington, 2003).

- Shaly-sandstone: - This contains clay minerals, which can be present as shale laminations, structural shale (load-bearing grains), and dispersed shale in the form of allogenic clay minerals (e.g. transported detritus) or authigenic clay minerals (e.g. cements or overgrowths).

1.5 Geologic Setting of Magnolia Field

The study location lies in the Magnolia field located in the Titan mini-basin approximately 180 miles south of Cameron, Louisiana, United States, in Garden Banks blocks 783 and 784 of Gulf of Mexico (see figure 1.2). Magnolia field was discovered in 1999 in about 4700 feet of water with the Garden Banks (GB) 783-1 well that was drilled in 4668 ft of water to a total depth of 16 867 ft (Weissenburger and Borbas, 2004).

The Magnolia field hydrocarbon-bearing reservoirs are Miocene, Pliocene and Pleistocene in age and were deposited from about 7.0 to 1.4 Ma ago. Magnolia reservoir materials are composed of silt-sized sediments that form a complex series of generally fining-upward channel/levee deposits (McCarthy *et al.* 2006). The siliciclastic material within the field were derived principally from the west, northwest and north through long lived submarine systems and deposited across a pronounced north-protruding salt nose that lies on the southern margin of the Titan mini-basin. Pliocene deposition was dominated by deep-water ponded facies

assemblages consisting of sheet sandstones and intervening mudstones (Prather *et al.* 1998).

The transition from Pliocene to Pleistocene deposition was marked in Magnolia by a significant unconformity characterized by a channel scour morphology. This separates Pliocene ponded facies from Pleistocene transitional facies, consisting of a stacked series of amalgamated channels, mudstones and lobe or sheet sandstones. These transitional facies are overlain by a (non-reservoir bearing) shale-dominated bypass facies assemblage that records a decrease in accommodation space relative to sediment influx during the latest Pleistocene (Weissenburger and Borbas, 2004).

Channels are defined as long-lived sediment pathways that are both erosional and depositional features (Lalande, 2002). Levee deposits are fine-grained laminated sandstones and can show the best porosity-permeability combination in the system. Over bank deposits are low sandstone/shale ratio intervals of the levees, so called “low pay, low resistivity sandstones” (Weimer *et al.* 1998 and Lalande, 2002). The Magnolia trap is formed by a combination of structural and stratigraphic elements such as dipping salt-detachment fault, channels and turbidite system. Magnolia hydrocarbon-bearing reservoirs lie within a depth interval extending from 12,600 to 16,800 ft true vertical depth (approximately 8,000-12,000ft below seabed). Additionally, as is typical of this portion of the northern Gulf of Mexico salt and mini-basin province, present day geothermal gradients from the seabed to trap are low, on average 1.0^{o} F/100 ft. Magnolia reservoir temperatures range from 130 to 165^{o}F. The degree of

overpressure is modest and varies between reservoirs, ranging from about 2200 to 5400 psi above hydrostatic (Weissenburger and Borbas, 2004).

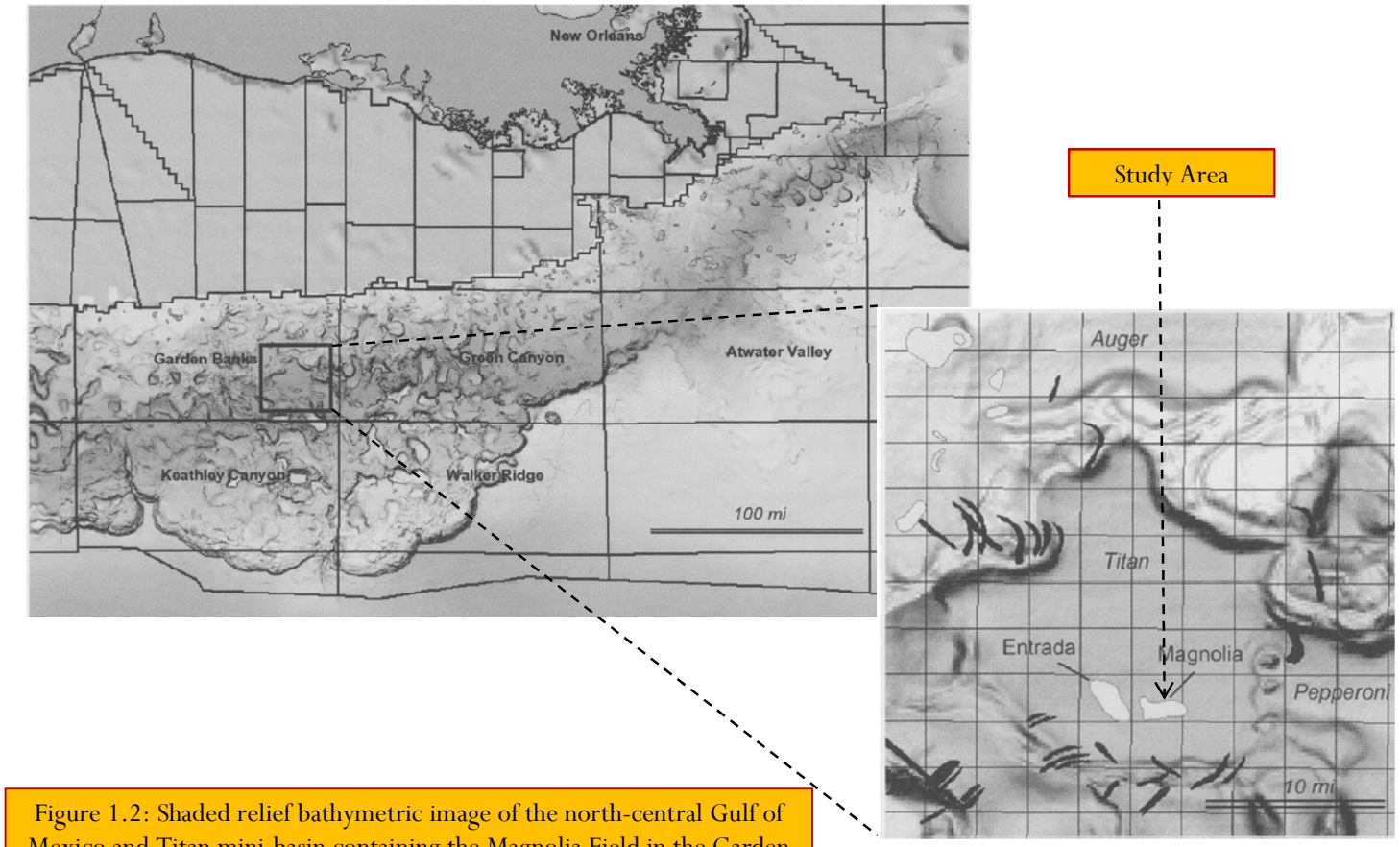

Figure 1.2: Shaded relief bathymetric image of the north-central Gulf of Mexico and Titan mini-basin containing the Magnolia Field in the Garden Banks Federal area (after Weissenburger and Borbas, 2004).

Table 1.1: Generalized geological model for Gulf of Mexico Cenozoic reservoirs

(Courtesy: Final Report - IOR for Deepwater Gulf of Mexico, 2010)

Generalized Geological Model for Gulf of Mexico Cenozoic Reservoirs		
	Characteristic	
1	Paleo-environment	Deltaic
2	Depositional model	Submarine fan system
3	Age of deposits	Neogene - Upper Cenozoic Paleogene - Lower Cenozoic
4	Regional controls	Salt canopy
5	Facies	Channel, sheet, lobe, and levee sands
6	Architecture	Fold belt, anticline, 3-way closure
7	Regional orientation	Northeast-southwest trending structures
8	Petroleum trap	Compressional fold, turtle structure, mini-basin, shale transition
9	Petroleum source rock	Upper Jurassic and Middle Cretaceous organic-rich carbonates
10	Formation lithology	Interbedded sandstones and shales
11	Reservoir targets	Neogene - Pleistocene (Quaternary), Pliocene, Miocene Paleogene - Oligocene, Eocene (Upper Wilcox), Paleocene (Lower Wilcox)
12	Reservoir rock	Turbidite sandstones
13	Texture	Neogene - coarse to fine grained; friable to consolidated Paleogene - fine-grained; consolidated
14	Mineralogy	Neogene - clean siliciclastics, some detritus Paleogene - siliciclastics, clay, and cement

CHAPTER 2

PETROPHYSICAL STUDY

2.1 Crossplots Analysis

Cross-plotting is a widely used technique in petrophysical and rock physics analysis as it enables a quick and meaningful evaluation of attributes with ease (Castagna *et al.* 1997; Oyetunji, 2013). Where core data are not available, it is sometimes helpful to plot certain parameters from well-log data for reservoir identification purposes i.e., gamma ray (GR) versus density (ρ_{bulk}). Figure 2.2a-c shows how cross-plotting technique is used in establishing the gamma-ray cut-off to discriminate reservoir form non-reservoir rocks. This technique is also useful in inferring grain-size distribution and rock sorting. In my area of study, the identification of the matrix components is well defined through the different crossplots displayed. The fundamental idea of such a technique is that different kinds of rock matrix are revealed by cross-plotting different well log parameters. The combined plot in this case includes; gamma ray versus sonic transit time (GR-ΔT), gamma ray versus density (GR-ρb), and gamma ray versus neutron porosity (GR-ΦN). By this concept, the rock types of the studied wells can be discriminated (Said *et al*. 2003). These crossplots assist in defining the different lithologies such as sandstones, shales, limestones and evaporates (Schlumberger, 1972). The qualitative interpretation of these crossplots is based on the transformation of the encountered log responses into the lithologic components and mineral constituents (Serra, 1986).

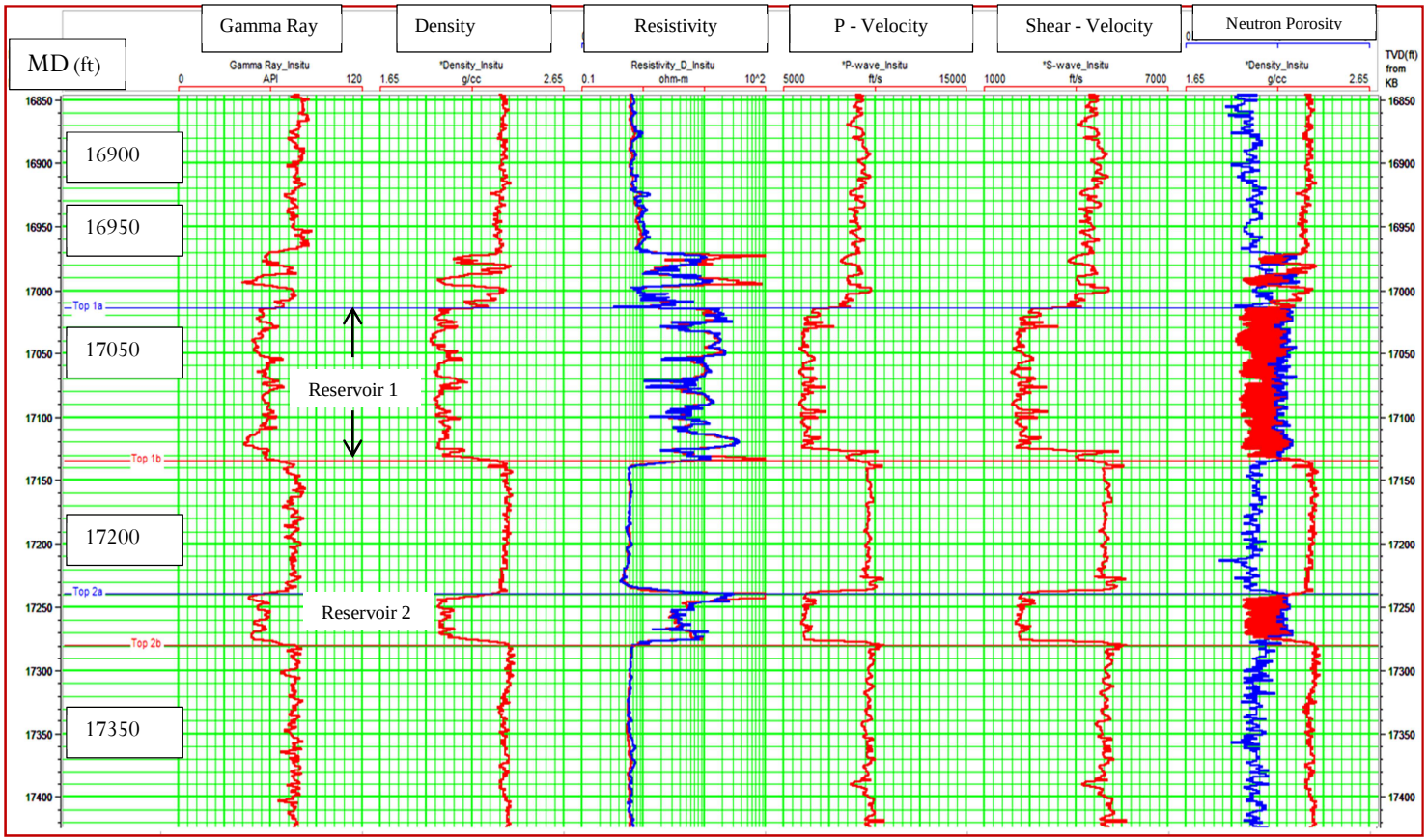

Figure 2.1: Log response at reservoir interval in well 6. The depths are in feet measured depth (MD). Displayed depth is between 16850 ft and 17440 ft.

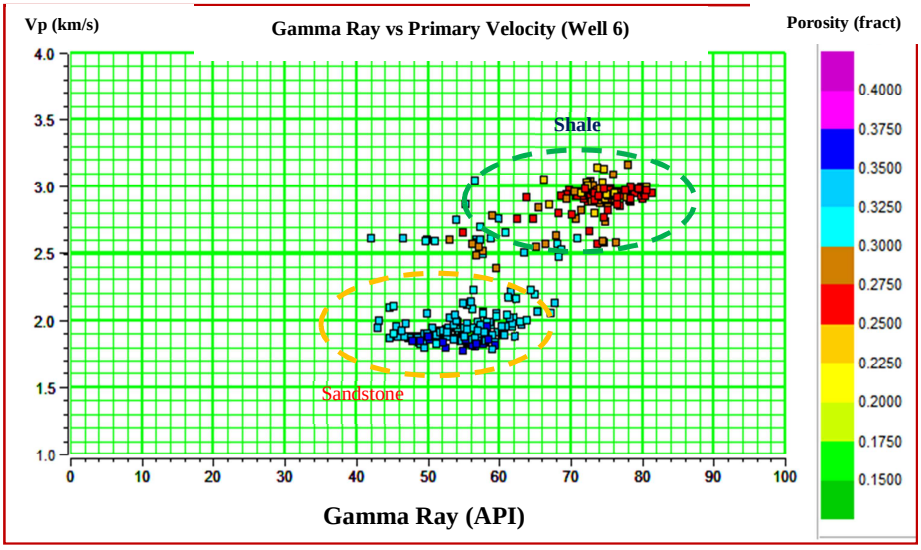

Figure 2.2a: Crossplot of gamma ray versus primary wave velocity color coded with porosity; orange dotted sphere indicate low gamma ray value at potential reservoir zone with corresponding low primary wave velocity. Higher gamma ray and corresponding higher velocity indicates non-reservoir zone.

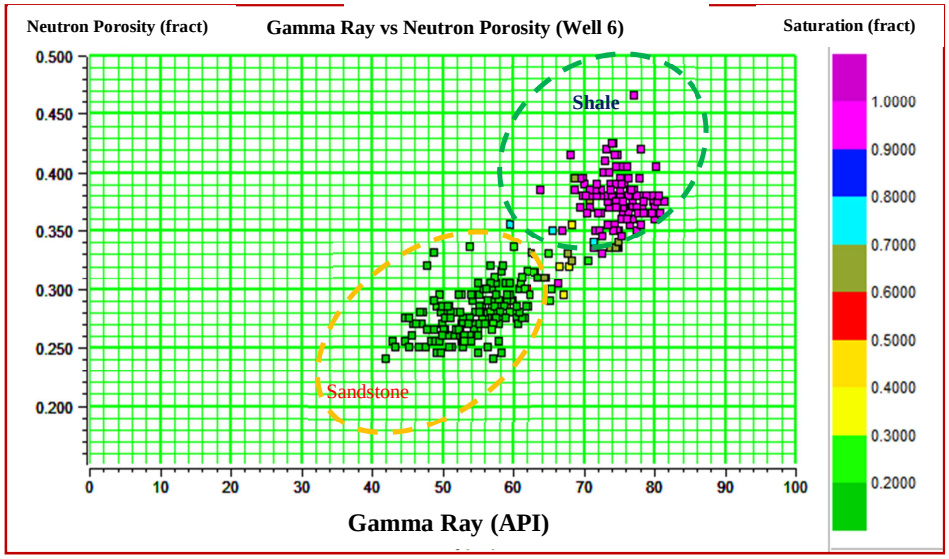

Figure 2.2b: Crossplot of gamma ray versus neutron porosity color coded with saturation; orange dotted sphere indicate low gamma ray value at potential reservoir zone with corresponding low neutron porosity value. Higher gamma ray and corresponding higher neutron porosity indicates non-reservoir zone.

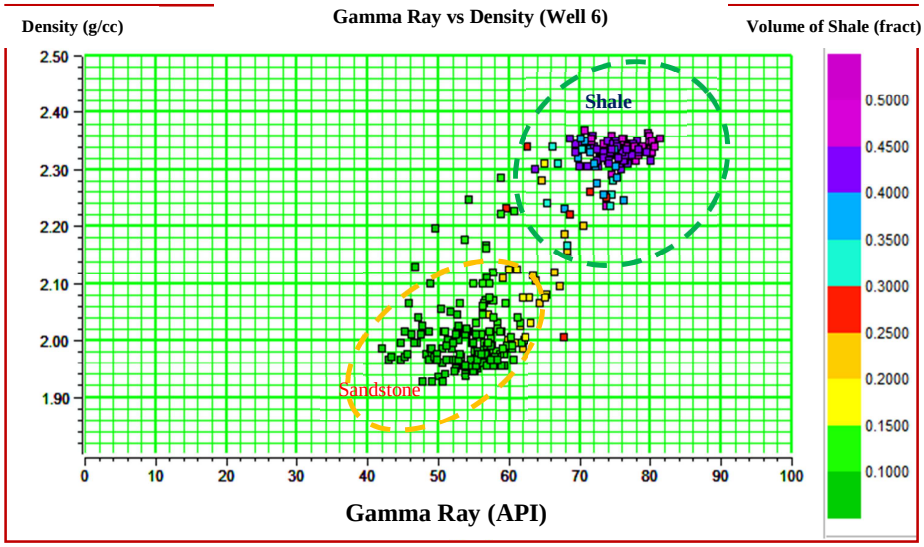

Figure 2.2c: Crossplot of gamma ray versus density color coded with shale volume; orange dotted sphere indicate low gamma ray value at potential reservoir zone with corresponding low density value. Higher gamma ray and corresponding high density indicates non-reservoir zone.

2.2 Logging Tools and Well- log Interpretation

For the purpose of quantitative interpretation, the first step in well-log analysis involves conditioning the logs for erroneous data points. This process involves plotting each log against depth to establish a trend. Data values that show abnormal deviation from this trend are considered outliers and are edited appropriately. Outliers may exist due to an enlarged region of a well bore known as washout or it may be due to cycle skip typically associated with more severe washouts or gas in drilling mud. Hydrocarbon-bearing reservoirs are identified both qualitatively and quantitatively. The qualitative analysis involves scanning through the well logs for hydrocarbon reservoir signatures such as low gamma ray, high resistivity, Cross-over of neutron and density logs (gas reservoirs), (see figure 2.1), while the quantitative method entails calculating for parameters such as shale volume, water saturation, and effective porosity. Gamma ray cut-off of 60 API was taken to decipher reservoirs from non-reservoirs.

2.2.1 Gamma Ray Logs

The gamma-ray log measures the amount of natural radioactivity of a formation. It is an excellent log used to distinguish sandstone from shale in clastic environments (Darling, 2005). Gamma rays are high-energy electromagnetic waves which are discharged by atomic nuclei inform of radiation. It measures the radiation originating from naturally occurring uranium, thorium, and potassium. Gamma ray log reflects shale or clay content. Clean sandstone formations have low radioactivity level and thus have low gamma ray readings while clay formations has high radioactive content

which explains its corresponding high gamma ray reading. Applicability of gamma-ray log ranges from correlation between wells, determination of formation boundaries, evaluation of clay volume within a formation, mineral analysis, seismic-well ties, side-wall coring, and or perforating.

From Figure 2.1, reservoir zones show low gamma ray and deflection to the left towards the lower values which indicate sandstone or shaly-sandstone formation. The values for gamma ray logs in clastic sediments vary from 0 – 150 API units, setting gamma ray cut off at 60 API where readings below 55 API indicate sandstone units, values above 55 API to 70 API indicate shaly-sandstone and values greater than 75 API indicate shale units. In Magnolia field wells, the lowest and highest readings on the gamma ray log are 32 and 118 respectively, and this is an indication that the sandstone reservoirs are young and unconsolidated, and the clay is over-pressured. Figures 2.1 and 2.4 shows the well-logs from well 1, i.e., upper and lower reservoir respectively; the upper reservoir interval is between 17,015ft – 17,135ft with lowest gamma ray values of 32 API units while the lower reservoir interval is from 17,240ft – 17,280ft with lowest gamma ray value of 35 API units. The same trend is observed in all other wells in Magnolia field, thus giving us an insight that the sandstones in Magnolia field are shaly-sandstones.

2.2.2 The Density Log

The density log measures formation's bulk density by injecting gamma rays into the formation through a process known as Compton scattering. These gamma rays are spotted by the detectors (Darling, 2005).The formation density log is an example of

porosity log that measures electron density of a formation. Dense formations produce large amount of gamma rays, while low-density formations produce fewer gamma ray. Hence, high-count rates at the detectors indicate low-density formations, while low count rates at the detectors signifies high-density formations.

Well 1 records a high density of about 2.40 g/cc in the shale unit at 14,565ft and decreases to about 1.92 g/cc in the sandstone reservoir at 14,071ft. Similar behavior is exhibited in other wells. Generally, low densities are observed in all sandstone units while the gas-saturated reservoirs record the lowest densities, which indicate the presence of hydrocarbons. The average density value for brine-saturated sandstone is about 2.25 g/cc. The neutron and density logs are good discriminator between gas and oil.

2.2.3 Neutron Log

The neutron logs measure formation's reaction to rapid neutron barrage which is related to the formation hydrogen index. The neutron logs respond to hydrogen in a formation and therefore the bound and structural waters conjoin with clay minerals are revealed as a heightened porosity value. Neutron log is used for gas detection; they generally have low values in gas reservoir regions. This is consequent to the fact that gas reservoir zones usually have low hydrogen content, thus we have neutron logs having a lower value.

2.2.4 Density Porosity and Neutron Porosity Logs

The combination of the neutron and density-log measurements is probably the most widely used porosity log combination especial for gas reservoir identification (Asquith, 2004). The curve pattern produced by the combination of these two logs is used for gas identification. Gas in the pores causes the density porosity to be too high (gas has a lower density than oil or water) and causes the neutron porosity to be too low (there is a lower concentration of hydrogen atoms in gas than in oil or water). Figure 2.1 and 2.3 shows an example of a gas zone. In that zone, the neutron porosity is less than the density porosity, and the two porosity curves cross over each other which suggest good gas saturation.

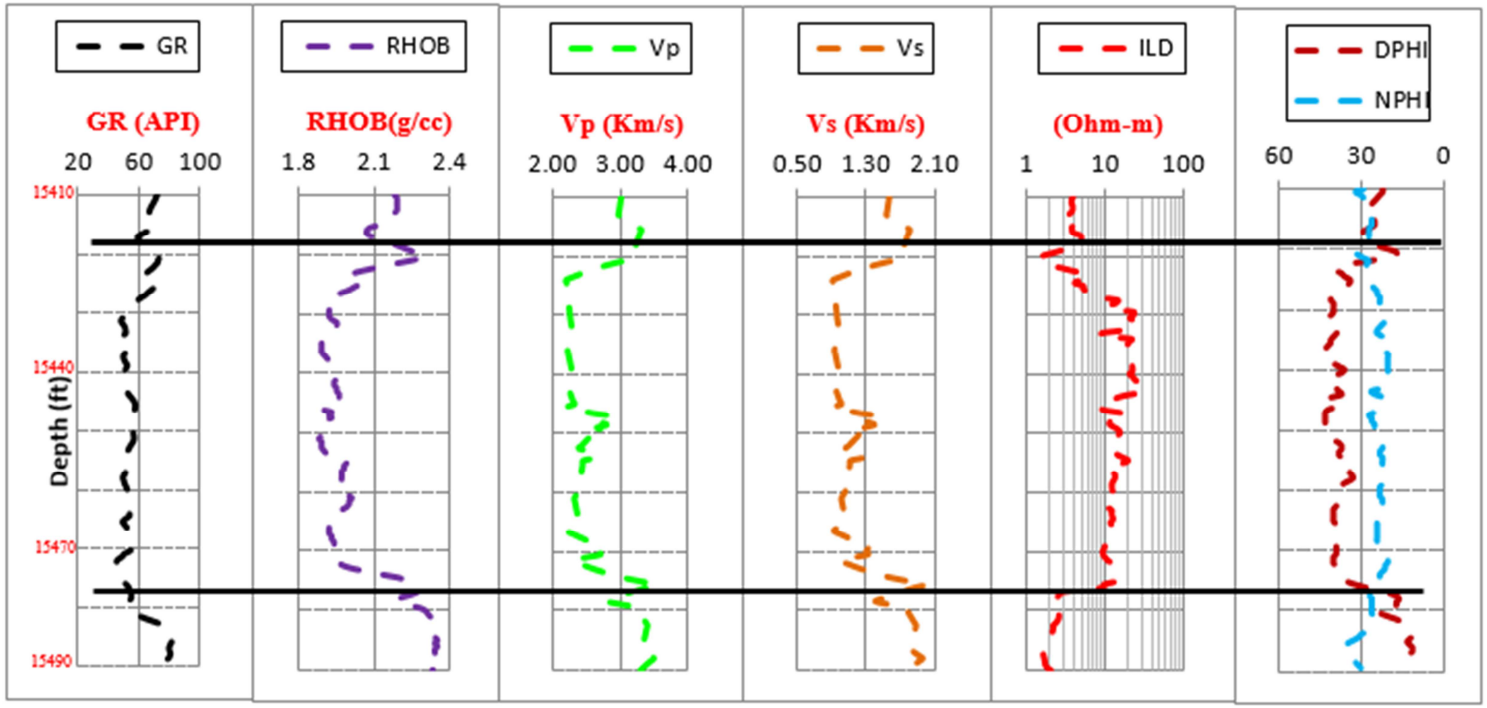

Figure 2.3: Composite log for well 4 showing a good cross over on neutron and density porosity log (black lines define the top and the base of the reservoir zone). Track 6 shows the density porosity log and neutron porosity log

Porosity is mathematically expressed as the ratio of pore space to total volume of rock;

$$\varphi = \left(\frac{Volume\ of\ Pore\ space}{Total\ volume\ of\ rock}\right) \times 100\% \qquad (1)$$

Where φ is the percentage porosity

However, due to the fact that density logging tools do not directly measure porosity, it is estimated as;

$$\varphi = \frac{\rho_{bulk} - \rho_{matrix}}{\rho_{fluid} - \rho_{matrix}} \qquad (2)$$

Where;

$$\rho_{bulk} = bulk\ density\ of\ the\ rock$$

$$\rho_{matrix} = density\ of\ the\ matrix$$

$$\rho_{fluid} = density\ of\ the\ fluid$$

$$\varphi = density - derived\ porosity$$

The density porosities are calculated by identifying bulk density (observed from the log), and the matrix density or grain density (quartz) of 2.65 g/cc was assumed for all calculation. Fluid density depends on the saturation of brine and hydrocarbons present in the invaded zone where bulk density tool measures.

2.2.5 Resistivity Log

Resistivity logs measure the capability of rocks to conduct electrical current or resist the flow of electric current. The scaled units are in ohm- meters. Resistivity is the inverse of conductivity and the rate at which a rock will conduct electric current will depend on the volume of water, the temperature of the formation and the salinity of the formation. A brine-saturated rock is expected to have a lower resistivity than hydrocarbon saturated rock because brine is more conductive. Resistivity logs interpreted at reservoir zones shows higher resistivity values compared to surrounding formation (see Figure 2.3 tracks 6 and Figure 2.4 tracks 5). The values of resistivity in the gas-saturated reservoir of Well 4 ranges between 20 and 40 ohm-m; 1 to 3 ohm-m in the surrounding shale and 0.3 to 0.7 ohm-m in brine-saturated sandstone formations. These resistivity values are used in the estimation of water saturation in the reservoir which will be discussed later.

2.2.6 Sonic Velocity Log

Primary wave sonic log measures the interval transit time (Δt in $\mu s/ft$) of a compressional sound wave travelling through one foot of formation (Darling, 2005). The value of transit time measurement within a formation is dependent on the lithology and the porosity of that formation. Primary wave velocity log measurement can be used in determining porosity of a consolidated formations, it is also very beneficial in other applications, such as: lithology indicator (using the ratio of primary velocity over shear velocity), detection of fractures and evaluation of secondary porosity, detecting over-pressure zones, determining mechanical properties, and

determining acoustic impedance for synthetic seismogram generation. In sandstones with constant porosity, clay minerals can cause a reduction in primary wave velocity, with the increasing effect been greater as small amounts of clay minerals are initially introduced and then declining with the introduction of additional clay mineral.

2.3 Quantitative Log Interpretation and Formation Evaluation

This involves quantitative estimate of reservoir parameters such as clay volume (lithology), effective porosity and water saturation.

The steps shown define the formation evaluation procedure adopted:

a) Determining the volume of clay in the formation (V_{cl})
b) Use the clay volume to correct total porosity (φ_t)values and estimate the effective porosity(φ_e)
c) Use the clay volume and effective porosity to determine the effective water saturation (S_{we})

2.3.1 Determining Clay Volume

Clay volume estimate was computed using the gamma ray log. The following equation defines the procedure:

a) Calculate the Gamma ray index (I_{GR})

$$I_{GR} = \frac{(GR_{log} - GR_{min})}{(GR_{max} - GR_{min})} \qquad (3)$$

Where;

$$I_{GR} = Gamma\ Ray\ index$$

$$GR_{log} = Gamma\ Ray\ reading\ from\ shaly\ sand$$

$$GR_{min} = Gamma\ Ray\ minimum\ from\ clean\ sand$$

$$GR_{max} = Gamma\ Ray\ maximum\ from\ shale$$

b) For unconsolidated Tertiary sand clay volume estimate:

$$V_{CL} = 0.83\left[2^{(3.7\times I_{GR})} - 1.0\right]\ (for\ unconsolidated\ sand)$$

2.3.2 Determining Effective Porosity

To estimate effective porosity (φ_e) for the shaly sand, two conditions were observed:

- If $\varphi_{nc} < \varphi_{dc}$, which indicates that the pore fluid is gas, the effective porosity is estimated as shown below;

$$\varphi_e = \sqrt{\frac{(\varphi_{dc}^2 + \varphi_{nc}^2)}{2}} \qquad (4)$$

- If $\varphi_{nc} > \varphi_{dc}$, which indicates that the pore fluid is water or oil, effective porosity is estimated as shown below;

$$\varphi_e = \frac{\varphi_{dc} + \varphi_{nc}}{2} \qquad (5)$$

Where φ_{nc} and φ_{dc} are the neutron and density porosity corrected for clay respectively.

Also the clay-correction equation for neutron porosity and density porosity are shown below;

$$\varphi_{dc} = \varphi_d - (V_{cl} \times \varphi_{dsh}) \quad (6)$$

$$\varphi_{nc} = \varphi_n - (V_{cl} \times \varphi_{nsh}) \quad (7)$$

Where φ_{dsh} and φ_{nsh} are the density and neutron porosity read in nearby shale zone.

φ_{nc} and φ_{dc} are the neutron and density porosity log of the zone respectively.

2.3.3 Determining Effective Water Saturation

Water saturation is an essential parameter used to estimate the volume of hydrocarbons in place, but is the most difficult parameter to accurately calculate. For laminated clay in the reservoir, Dual water model approach was adopted.

To estimate the water saturation corrected for clay effect:

Recall equation for effective porosity estimate;

- **Calculate total porosity of adjacent shale(φ_{tsh}).**

$$\varphi_{tsh} = \varphi_{dsh} + \varphi_{nsh} \quad (8)$$

Where φ_{dsh} and φ_{nsh} are the density and neutron porosity read in nearby shale zone.

- **Calculate total porosity (φ_{tsh})and bound water saturation (S_b)**

$$\varphi_t = \varphi_e + V_{cl}\varphi_{tsh} \quad (9)$$

$$S_b = V_{cl} \times \varphi_{tsh}/\varphi_t \quad (10)$$

Where;

$$S_b = clay\ bound\ water\ saturation$$

$$\varphi_t = total\ porosity$$

$$\varphi_e = effective\ porosity$$

$$V_{cl} = volume\ of\ clay$$

$$\varphi_{tsh} = total\ porosity\ of\ adjacent\ shale$$

- **Calculate bound water resistivity (R_b) from adjacent shale**

$$R_b = R_{sh} \times \varphi_{tsh}^2 \quad (11)$$

Where;

$$R_b = bound\ water\ resistivity$$

$$R_{sh} = Resistivity\ of\ adjacent\ shale$$

- **Calculate apparent water resistivity (R_{wa}) in the shaly sand**

$$R_{wa} = R_t \times \varphi_t^2 \quad (12)$$

Where;

$$R_{wa} = Apparent\ water\ resistivity$$

$$\varphi_t = total\ porosity$$

$$R_t = deep\ formation\ resistivity$$

- **Calculate total water saturation (S_{wt}) corrected for clay**

$$S_{wt} = b + \sqrt{b^2 + (R_w/R_{wa})} \quad (13)$$

Where;

$$S_{wt} = Total\ water\ saturation\ corrected\ for\ clay$$

$$b = [S_b(1 - R_w/R_b)]/2$$

$$R_w = Formation\ water\ resistivity$$

$$R_{wa} = Apparent\ formation\ water\ resistivity$$

- **Calculate effective water saturation (S_{we}) of the shaly sand**

$$S_{we} = (S_{wt} - S_b)/(1 - S_b) \qquad (14)$$

$$S_{we} = Effective\ water\ saturation$$

$$S_{wt} = Total\ water\ saturation$$

$$S_b = Clay\ bound\ water\ saturation$$

2.4 Results and Discussion

Based on the petrophysical analysis earlier described, reservoir zones were identified (see Figure 2.4 and Figure 2.5). The reservoir zones are characterized with low gamma ray, low density, high resistivity, low primary velocity, low shear velocity, low clay volume, low water saturation and high porosity. The anomalous region was interpreted as hydrocarbon-bearing intervals as it clearly shows fluid response. To buttress this result, fluid substitution modelling will be discussed in later chapters.

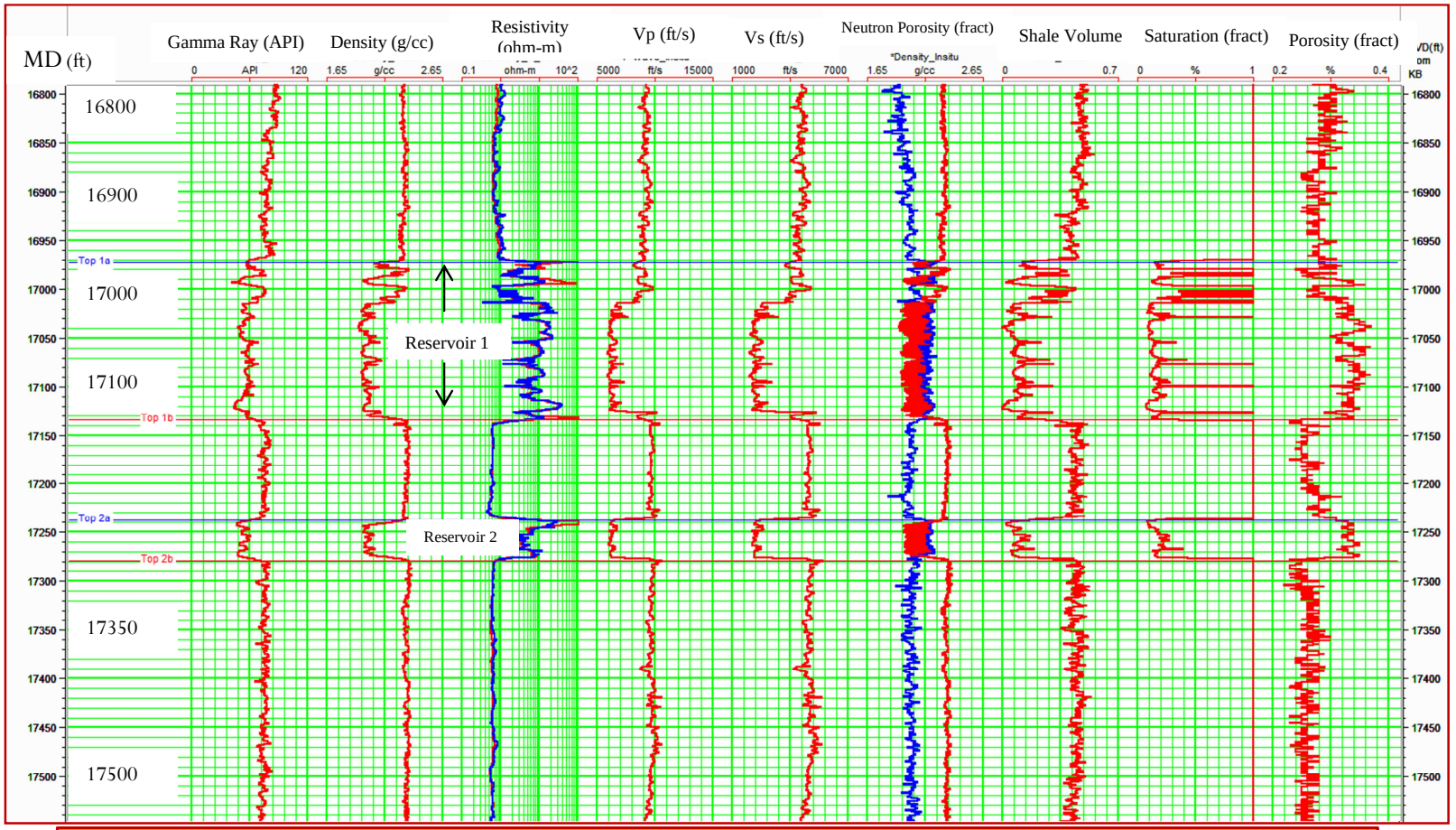

Figure 2.4: Quantitative log interpretation response at well 6. The depths are in feet measured depth (MD). Displayed depth is between 16800 ft and 17500 ft.

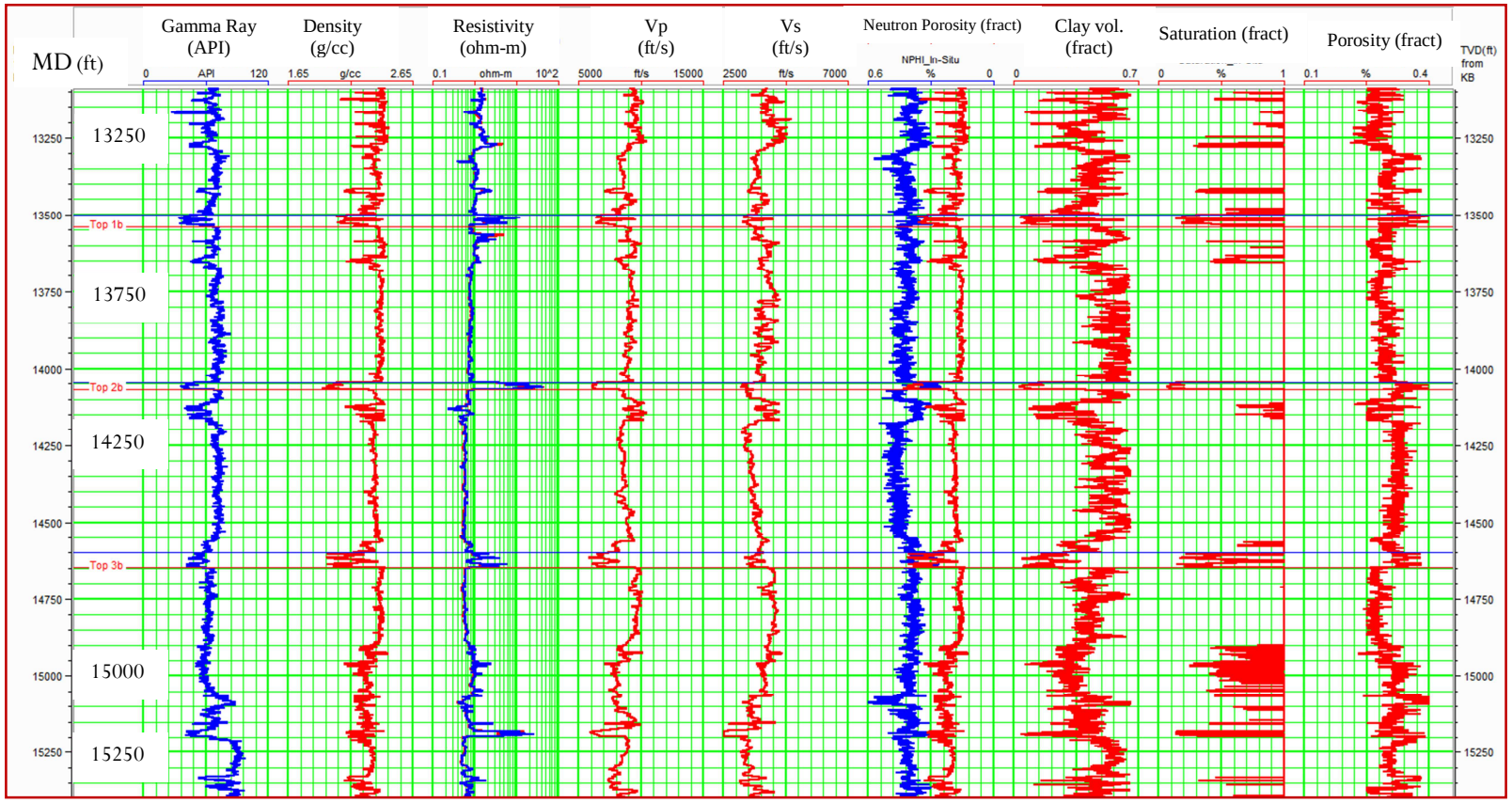

Figure 2.5: Quantitative log interpretation response at well 1. The depths are in feet measured depth (MD). Displayed depth is between 13100 ft and 15350 ft.

CHAPTER 3

ROCK PHYSICS ANALYSIS

3.1 Introduction

Rock physics establishes relationships between the physical rock properties and seismic parameters such as velocity, density, and attenuation. The discipline accounts for the solid rock frame (mineralogy, porosity, and pore shape and size), pore fluid (fluid type and saturation), pressure, and temperature. Generally, elastic properties of rocks are controlled by lithology (composition and texture), porosity (amount and type), pore fluids, depth (differential pressure, temperature, age and lithification), anisotropy, etc. (Table 3.1). The parameters in table 3.1 do not have the same importance, and the main controlling parameters can be, and usually are, different in different geologic environments.

Table 3.1: Factors controlling seismic properties in sedimentary rocks (Wang, 2001)

Rock properties	**Fluid properties**	**Environment**
Compaction	Viscosity	Frequency
Consolidation	Density	Stress history
Age	Wettability	Depositional environment
Cementation	Fluid composition	Temperature
Pore Shape	Phase	Reservoir process
Bulk density	Fluid type	Production history
Clay content	Gas-oil, gas-water ratio	Layer geometry
Anisotropy	Saturation	Differential pressure
Porosity		
Lithology		

3.2 Rock-Physics Models Overview

To predict effective elastic moduli of a combination of grains and pores, one need to specify volume fractions of each constituents, grain and pore arrangements, and elastic moduli of the constituents (Mavko *et al.* 2009). In order to predict velocity of a rock with known porosity, mineralogical composition and elastic moduli of mineral constituents, and having no information about grain and pore arrangements, the most suitable way is to use the upper and lower bounds of elastic moduli (Mavko *et al.* 2009).

Well logs provide data about constituents of formation and their volume fraction, while they provide relatively little information about grains and pore structures. Also, there is a minimum amount of *a priori* information that is required as a geological constrain on modelling:

- Lithology: a siliciclastic environment in the particular case at the Magnolia field, represented by clean sandstones, shaly-sandstones and shales;
- Pressure regime: the water depth and burial depth determine confining, pore, and effective pressure;
- Area/basin characteristics: which are related to shale-trend selection (gamma-ray reading) in a particular basin;

For this thesis work, various models were used to investigate reservoirs encountered in Magnolia field. The Thomas and Stieber (1975, 1977) model (TS) described the porosity-shale volume (Vsh) relations in clastic sediments i.e., volumetrics , the Yin (1992) and Marion (1990) developed an analogous clastics model (YM) for the elastic properties of clastic sediments composed of sandstone and shale end members based on laboratory measurements on sand-kaolinites, and Marion

(1990), Dvorkin and Gutierrez (2002) showed how to model (MDG) velocity vs. porosity by combining the TS model for porosity – shale volume and the YM model for velocity – shale volume. Gassmann's equation was employed in calculating elastic moduli at different saturation condition (theoretical model) of the reservoirs.

3.2.1 Theoretical Bounds

Theoretical bounds establish the physical limits of the properties of mixtures of minerals and fluids. Bounds are robust and free of approximations, other than to treat the rock as an elastic composite. They are valuable mixing laws. The lower bound is determined by Reuss average (describing a suspension of mineral and fluid) and the upper bound by a modified Voigt bound. Most often used are Voigt-Reuss and Hashin-Shtrikman bounds.

The Voigt and Reuss bound bounds are defined, for example with a mix of quartz and water, as follows,

Voigt modulus:

$$K_{Voigt} = \left(K_{qtz} * Vol_{qtz}\right) + (K_w * Vol_w) \qquad (15)$$

Where

$$K_{qtz} = modulus\ of\ quartz$$

$$K_w = modulus\ of\ water$$

$$Vol_{qtz} = Volume\ fraction\ of\ quartz$$

$$Vol_w = Volume\ fraction\ of\ water$$

Reuss modulus (describing a lower bound for mineral/fluid suspensions):

$$K_{Reuss} = \frac{1}{\frac{Vol_{qtz}}{K_{qtz}} + \frac{Vol_w}{K_w}} \quad (16)$$

The modified Voigt or Critical porosity model (Nur et al., 1998) provides a more realistic upper bound for sandstones and is defined by:

$$K_{mod\_voigt} = \left(1 - \frac{\emptyset}{\emptyset_c}\right)\left(K_{qtz} - K_{\emptyset c}\right) + K_{\emptyset c} \quad (17)$$

Where $K_{\emptyset c}$ is the Reuss modulus at critical porosity.

3.2.2 Thomas – Stieber Model

Thomas and Stieber (1975, 1977) explore quantitatively with a simple mathematical model how porosity could vary with shale volume depending on the configuration and distribution of shale in the sandstone – shale sequence. This model is fruitful for reservoirs which are found in Tertiary sandstone – shale sequences and usually will not apply to more complicated mineralogies involving carbonates.

The effects of clay geometry on measured petrophysical parameters are essentially fourfold. Firstly, the size and distribution of constituent clays and clay minerals have an abstruse influence on intergranular permeability. Secondly, the presence of microporosity within clay – mineral overgrowths on quartz and other detrital minerals lowers the formation resistivity and thereby increases the log-derived water saturation. Thirdly, the two effect mentioned above can cause high capillarity. Finally, clays and clay minerals when present as shale laminars within a sub-resolution sand-shale sequence can cause deep resistivity logging tools to under-read in the sandstones, where the measured deep formation resistivity can be typical of water-bearing rock even though the sand lamiae actually produce dry hydrocarbon

(Worthington, 2003). Also, there are three broad categories which describe how shale can be distributed in sand (figure 3.1) and of course there can be any combinations of these categories;

1. **Dispersed:** The clay mineral fills the intergranular space i.e. it changes the porosity leaving the matrix density untouched.
2. **Laminated:** These layers of clay in the matrix replacing both matrix and porosity, there are hence changes in matrix density and porosity.
3. **Structural:** Clay grains replace some of the sand grains, in this case the matrix density changes but the porosity does not alters.

There are five assumptions made in the Thomas – Stieber model:

- There are only two types of materials present; high porosity “clean” sandstone and low porosity “pure” shale.
- Within the interval investigated, there are no changes in shale type and the shale mixed in the sand is mineralogically the same as the “pure” shale sections above and below the sand.
- The gamma ray responds to the number of radioactive events in a material and thus it mass. The shale fractions we wish to determine are a function of volume. The assumption for Tertiary basins is that both sandstones and shales have comparable grain densities, thus, the radioactivity will be proportional to volume.
- Constant background radiation is assumed to be present in all measurements.
- Counting yields from the gamma ray don’t change as rock types are intermixed.

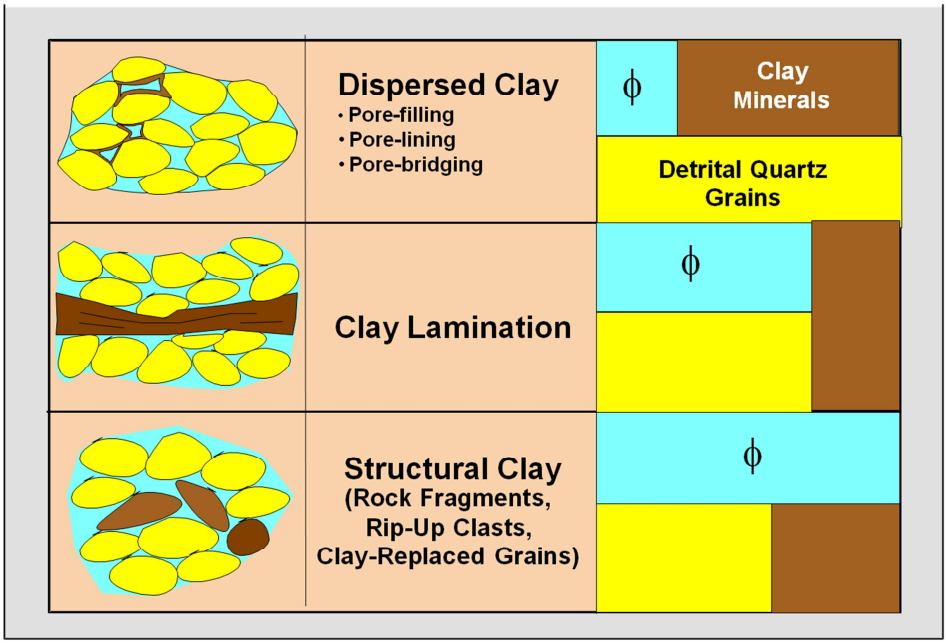

Figure 3.1: Common clay mineral distribution pattern

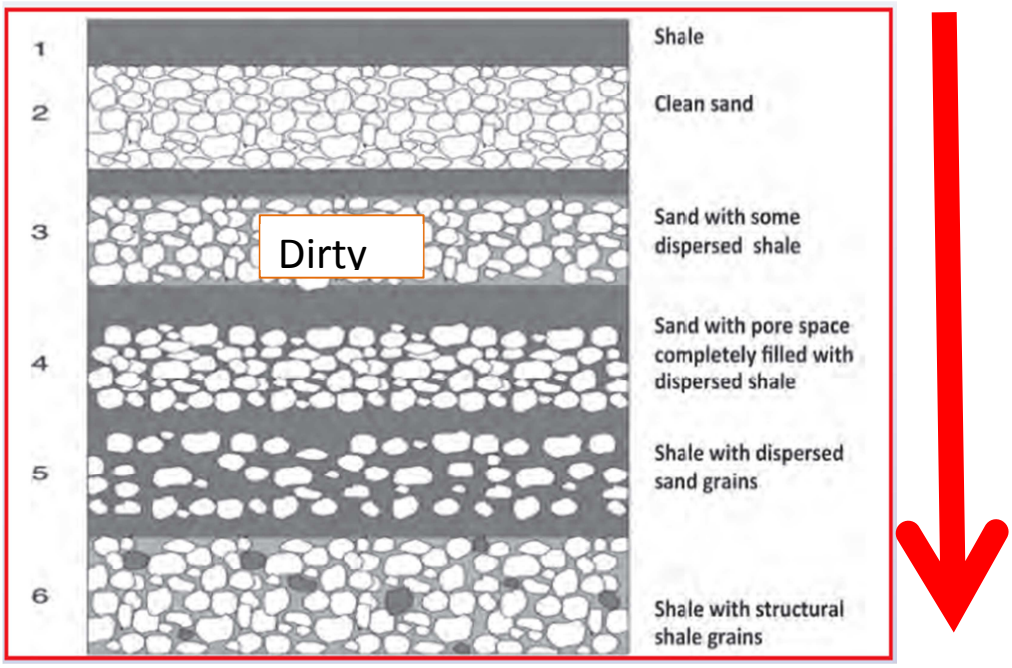

Figure 3:2: Various sandstone-shale mixtures within the Thomas-Stieber model (Modify after Mosab et al., 2012).

For simplicity, the Thomas – Stieber model agrees that shale is the main destroyer of sand porosity and it is therefore reasonable to expect the gamma ray to correlate to porosity. Figure 3.2 illustrates some of the lithologies considered in Thomas – Stieber model.

The explanation to figure 3.2 is as follows:

- Row labelled 1: Pure shale porosity $\emptyset_{shale}$ as one end-member
- Row labelled 2: clean sand porosity $\emptyset_{clean-sand}$ as the second end-member
- Row labelled 3: These illustrate a dirty sand scenario when shale is dispersed or lies within the original sand pore space. As long as the volume of shale Vsh is less than $\emptyset_{clean-sand}$ i.e. Vsh < $\emptyset_{clean-sand}$, the model assumes that the sand grain packing is undisturbed
- Row labelled 4: This is the extreme case of row 3 in which volume of shale (Vsh) equals clean sand porosity ($\emptyset_{clean-sand}$). At this point, the original pore space of sand is completely filled with shale.
- Row labelled 5: If we continue to add shale into the mixture, it is equivalent of replacing void-less sand grains by shale with porosity. Row 5 has shale fractions 1≤ Vsh ≤$\emptyset_{clean-sand}$, so that the sand grains are floating in the shale.
- Row labelled 6: A special case in which sand grains in Rows 2, 3, or 4 are replaced by structural shale clasts.

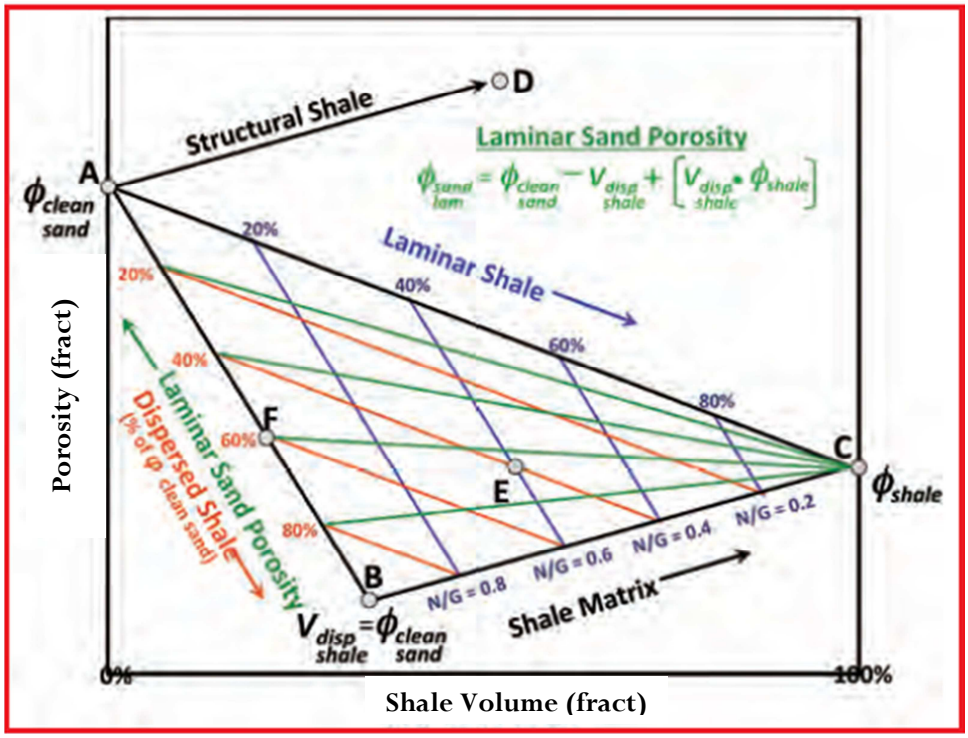

Figure 3.3: Total porosity vs. shale volume, as predicted by the Thomas-Stieber model. (After Mosab et al., 2012)

What we have in Figure 3.3 is a plot of porosity-shale relations as predicted by the Thomas-Steiber model. The shale distribution and porosity can be computed from Thomas-Stieber cross-plot, in which Volume of shale is plotted on X-axis and total porosity on Y-axis. Based on the position of the data points in this cross plot, laminar (V_{lam}), dispersed (V_{dis}), structural (V_{st}) shale volumes and porosity of sand laminae can be calculated using following equations.

1. Laminated shale only ($V_{sh} = V_L$)

$$\varphi_{total} = \varphi_{clean\ sand} - V_L\ (\varphi_{clean\ sand} - \varphi_{shale}) \qquad (18)$$

2. Dispersed shale only ($V_{sh} = V_D$)

$$\varphi_{total} = \varphi_{clean\,sand} - V_D\,(1 - \varphi_{shale}) \qquad (19)$$

3. Structural shale only ($V_{sh} = V_S$)

$$\varphi_{total} = \varphi_{clean\,sand} + V_S\,(\varphi_{shale}) \qquad (20)$$

4. Material balance for shale

$$V_{shale} = V_L + V_D + V_S \qquad (21)$$

Point A is the clean sand (> 90 % clean sand); C is the shale (> 90 % shale). Line A-B shows the trend of increased dispersed shale (lithologies 2-4 in Figure 3.2). Line B-C shows the trend of silt/sand grains replaced with shale matrix (lithology 5). Constant values of sand lamination porosity are defined by lines radiating from C. Depending on the local geological set-up it was assumed that amount of structural shale is too small to reduce the variable and simplify the shale distribution.

3.2.3 Dvorkin and Gutierrez Model

Dvorkin and Nur, 1996 investigated and identified that the gradient of velocity – porosity trend in clastic environment is highly variable and it thus depend largely on the geologic process that is controlling porosity. Porosity variations can be attributed to variations in sorting and clay content which tend to yield much flatter velocity – porosity trends. Porosity controlled by sedimentation or depositional process is generally expected to yield flatter trends. Figure 3.4 showed the generalized velocity – porosity model for clastic environment (Dvorkin and Gutierrez, 2002; Nasser, 2012). Sediments are deposited along the suspension line. Clean, well – sorted sands will

have initial (critical) porosity of ~0.4. Poorly sorted sediments will have a smaller critical porosity. Burial, compaction and diagenesis move data off the suspension line. The suspension line from the figure 3.4 is computed using the Reuss average of the mineral and pore fluid moduli and is a lower bound. The clean sand line is computed using a modified Voigt average trending between the clean sand critical porosity (φ_c=0.4 in this case) and pure mineral at φ = 0 (Dvorkin et al., 1991; Dvorkin and Nur, 1996). It should be noted that the modified Voigt is slightly steepened near critical porosity to reflect the rapid stiffening when new sediments are initially compacted and / or cemented.

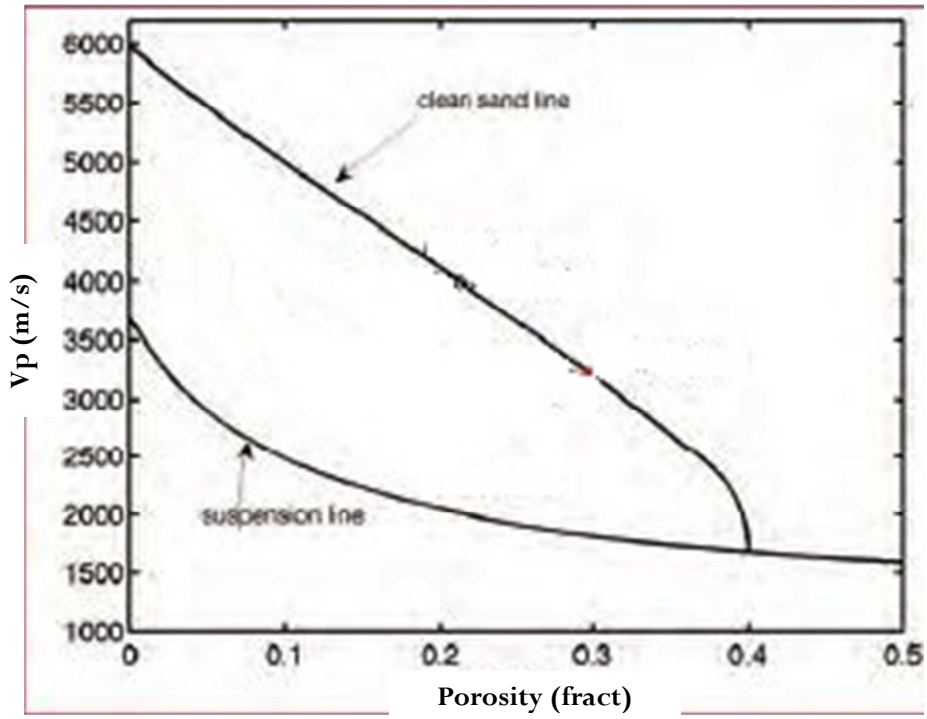

Figure 3.4: Velocity vs. porosity, as predicted by the Dvorkin-Gutierrez model. (Modified after Mosab et al., 2012)

3.3 Application Of the Thomas–Steiber Model On Field Data

The Thomas-Stieber model was used to investigate clay distributions at Magnolia field. On the Thomas-Steiber model diagram, the clean sandstone and pure shale points are those of above 90% sand (sand point A) and of above 90% shale (shale point C). In principle, the points are manually moved on the plot to be able to centre them on the sand and shale end points. Figure 3.5 to 3.7 show the various Thomas-Steiber plots from well 1 and 6 where shale volume was plotted against porosity, the figure shows how well data were super-imposed on the ternary diagram. The average sandstone porosity in Magnolia field ranges between 32% - 38% while the shale porosity is of the average of 28% - 32%. Figure 3.6 show the shale distribution observed in well one, three reservoirs were delineated with about 20 – 35% shale laminae, reservoir one and reservoir three shows more consequential influence on clay lamination but its influence is less pronounced compared to having dispersed clay presence. For example, the permeability of clean sandstone having 35% can be reduced to zero if its pores are filled with dispersed clay. But, if the same amount of clay is present in the laminated form, about two third of its permeability is still retained in the rock (Nasser, 2012). Figure 3.5 is the result obtained from well 6, the reservoir intervals R1 and R2 were matched with the Thomas-Stieber cross-plot superimposed with well data. The reservoirs are cleaner at both R1 and R2 with lesser percentage (about 15%) of laminated clay especially at reservoir R2

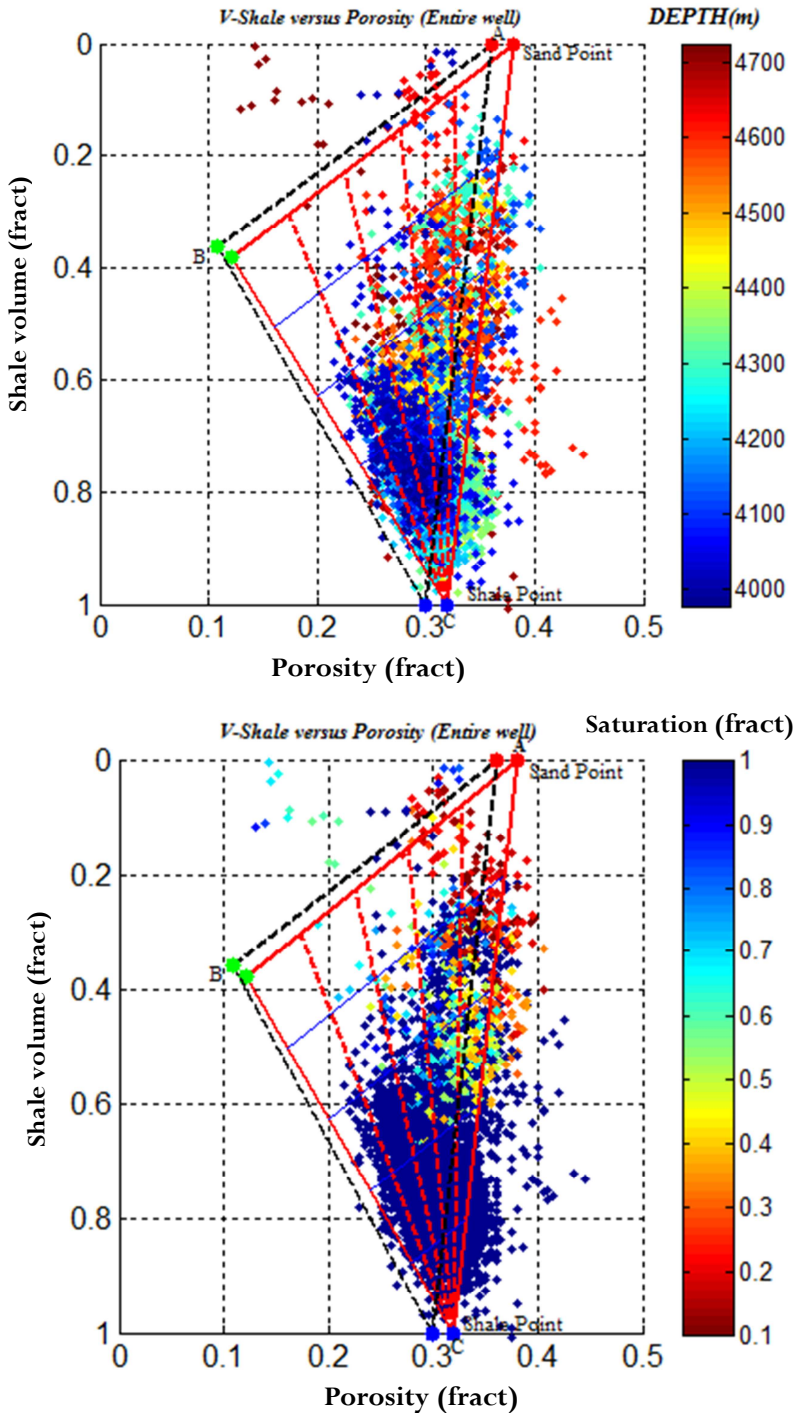

Figure 3.5: Crossplots of shale volume versus porosity with the Thomas-Stieber model super-imposed on the data from entire well 1 colour-coded with water saturation and depth

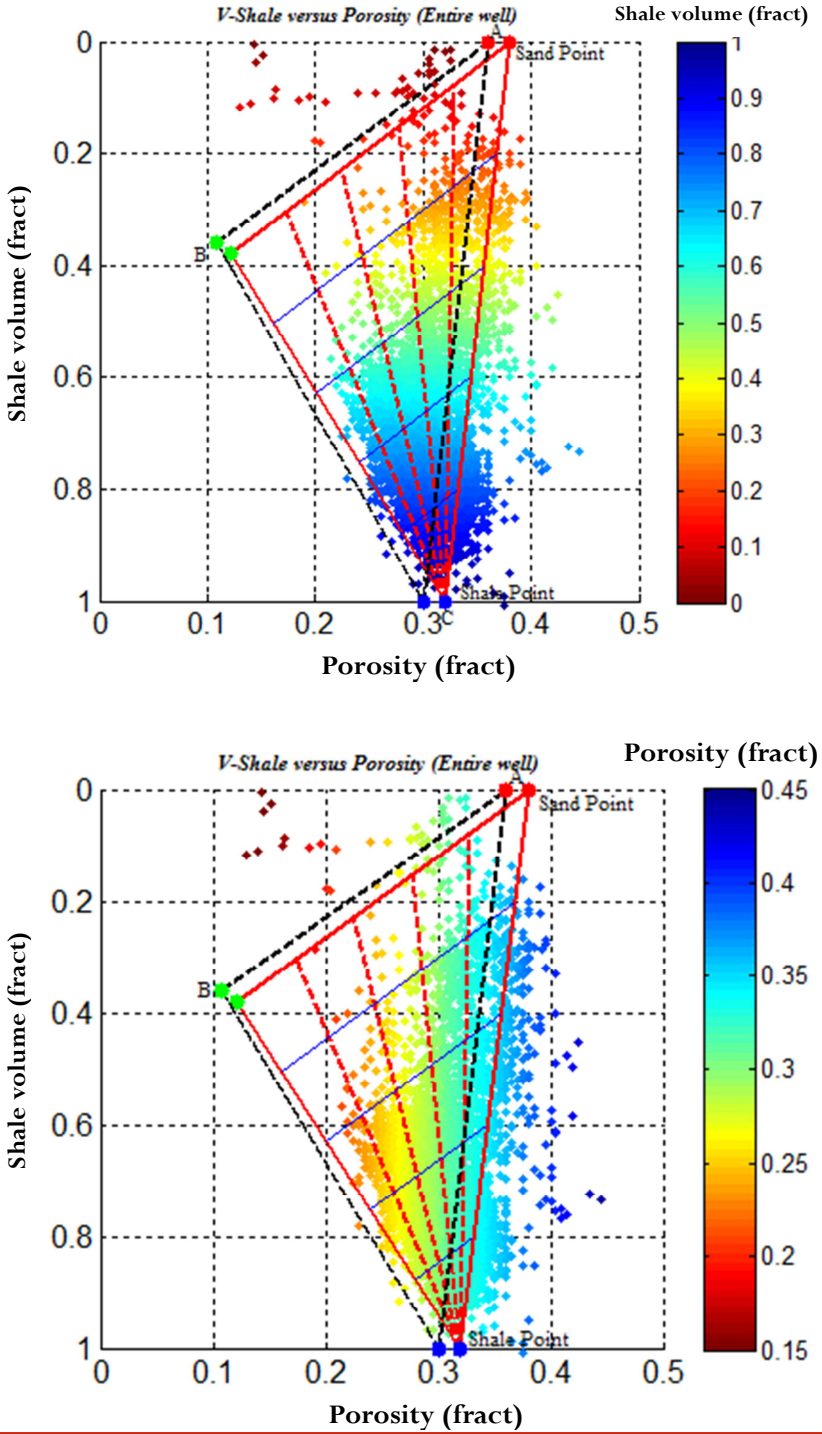

Figure 3.6: Crossplots of shale volume versus porosity with the Thomas-Stieber model super-imposed on the data from entire well 1 colour-coded with shale volume and porosity

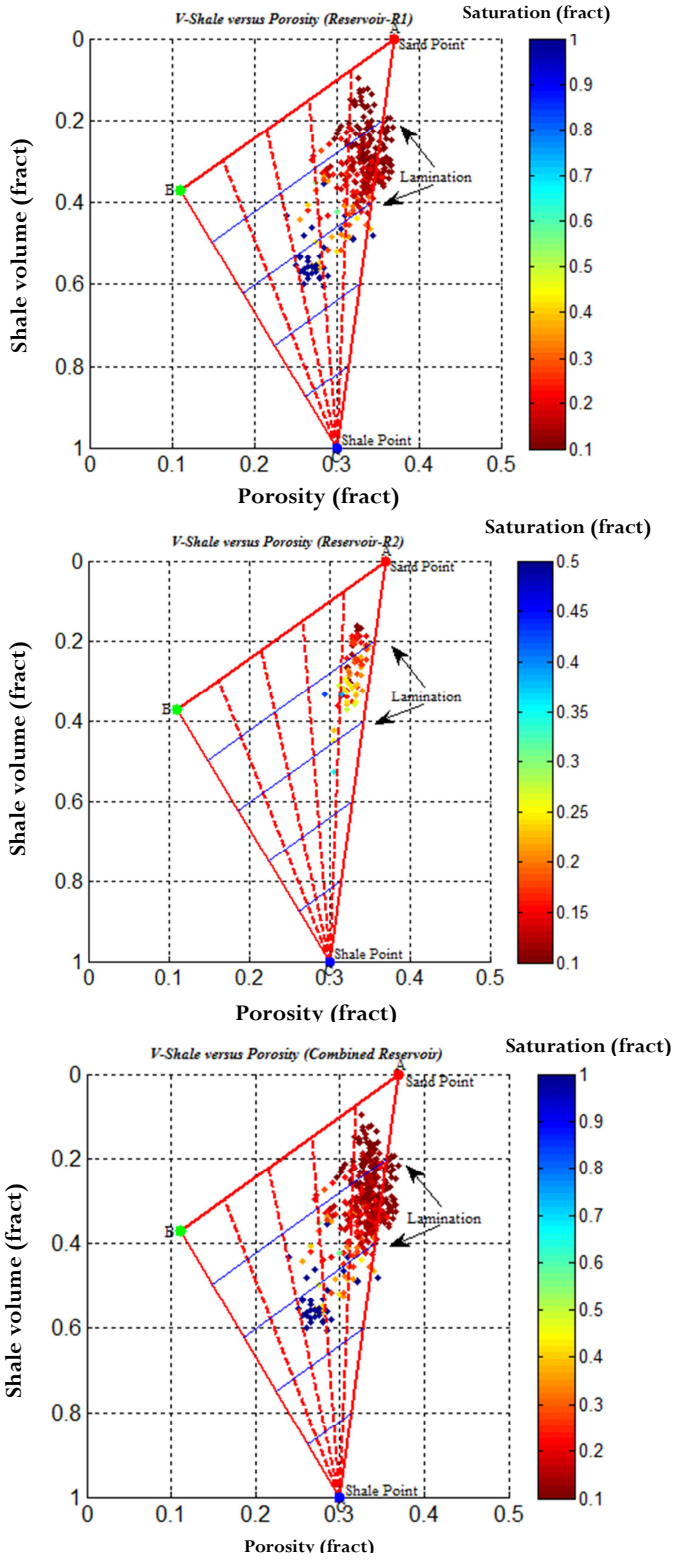

Figure 3.7: Crossplots of shale volume versus porosity with the Thomas-Stieber model super-imposed on the data from well 6 colour-coded with water saturation at reservoirs R1, R2 and Combination of R1 and R2

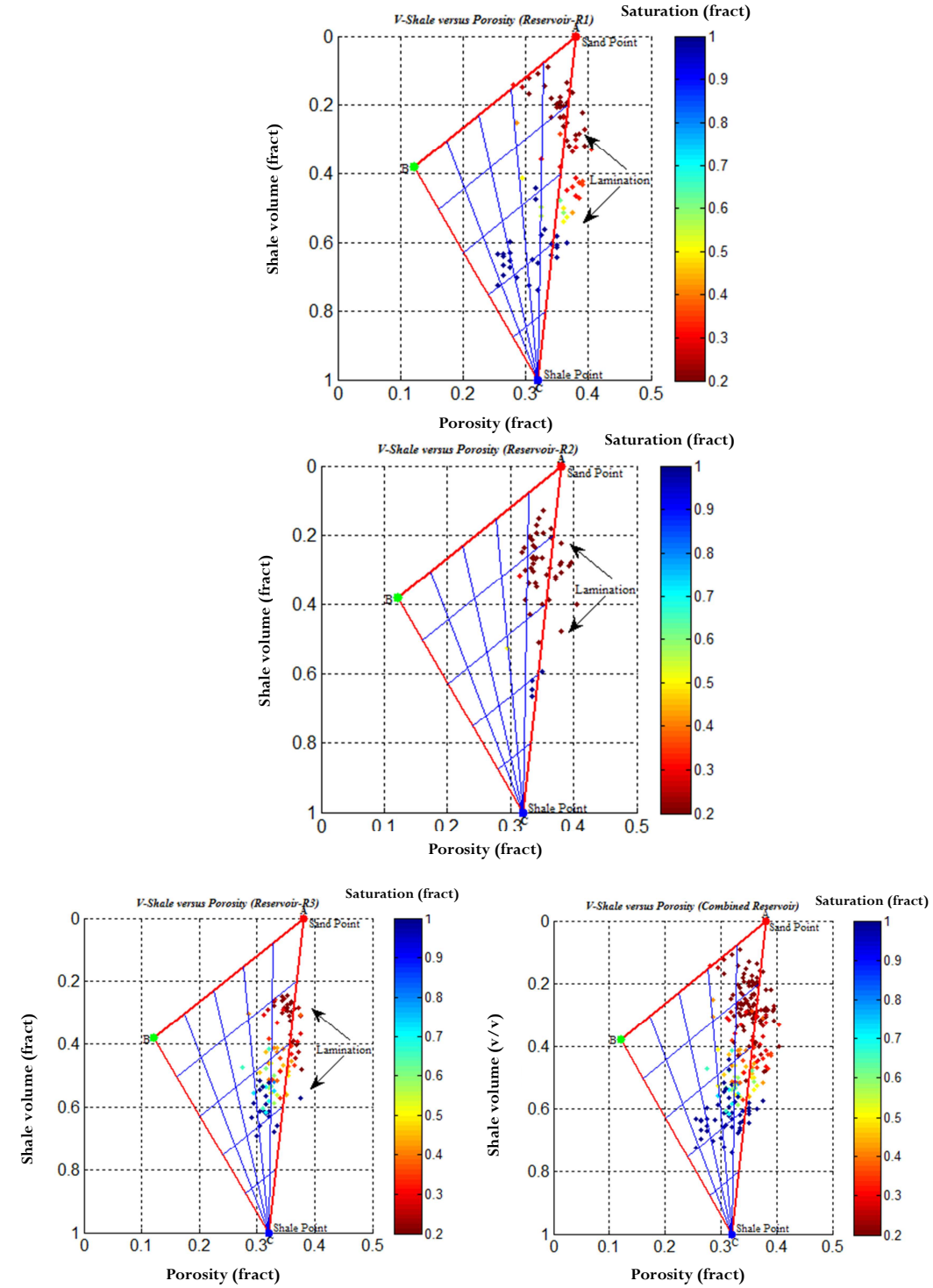

Figure 3.8: Crossplots of shale volume versus porosity with the Thomas-Stieber model super-imposed on the data from well 1 colour-coded with water saturation at reservoirs R1, R2, R3 and Combination of R1, R2 & R3

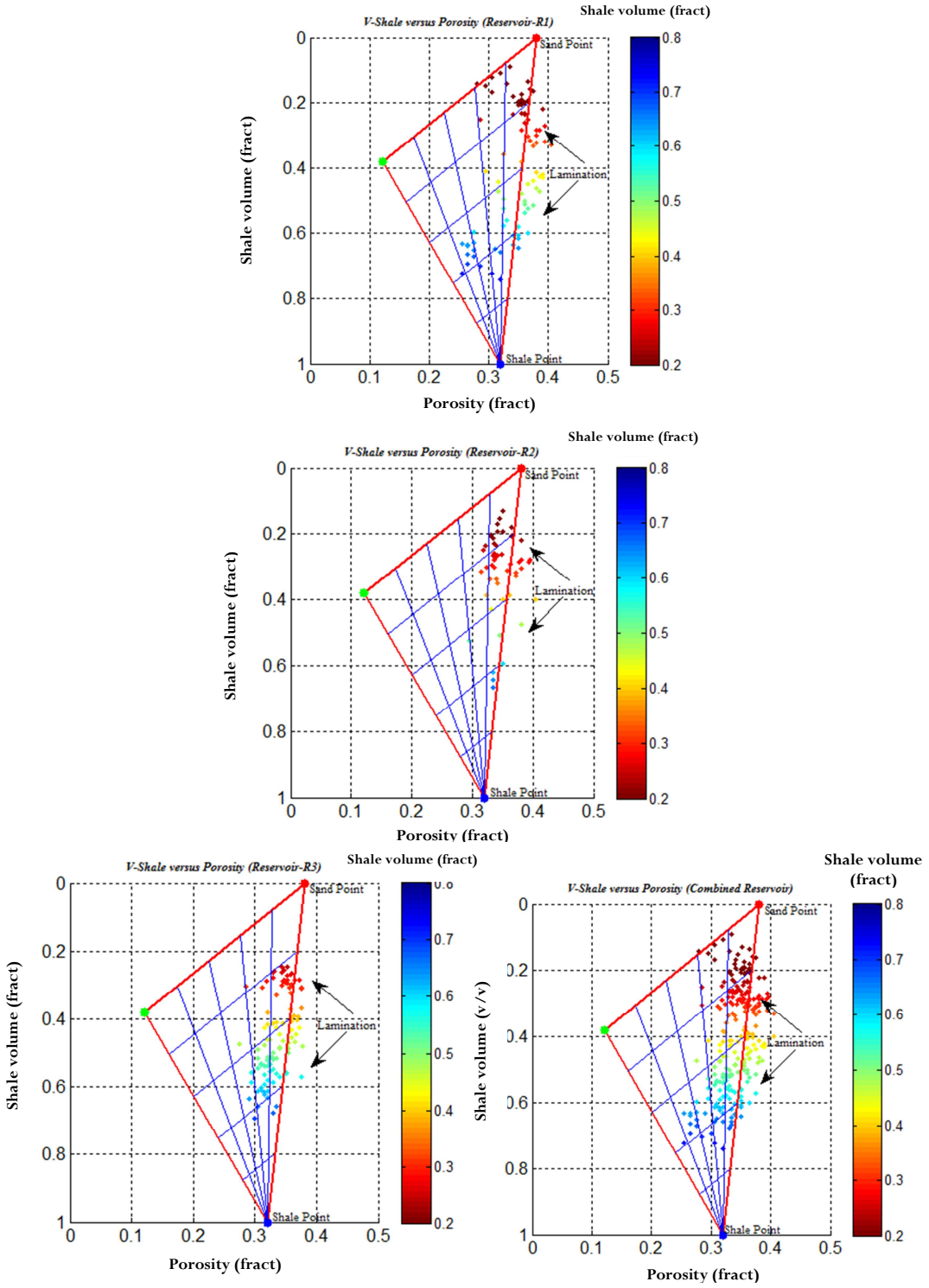

Figure 3.9: Crossplots of shale volume versus porosity with the Thomas-Stieber model super-imposed on the data from well 1 colour code with shale volume

3.4 Thomas-Stieber & Dvorkin-Gutierrez Model On Field Data

Figure 3.10 – 3.18 shows the hybrid model that was obtained through coupling the Thomas-Stieber model and Marion-Dvorkin-Gutierrez model. Porosity-velocity-shale lithologies are computed from the models in terms of the end members. Independent variables are the end member sand and shale properties, ($\phi_{clean\text{-}sand}$; $V_{clean\text{-}sand}$) and (ϕ_{shale}; Vshale). In a velocity versus porosity plane as plotted in Figure 3.8 - 3.17, well log data superimposed on the models shows a narrow spread which implies that the reservoirs in Magnolia field are young, unconsolidated and over-pressured. The interval observed is about 600ft for well 6 and about 1,200ft for well one. Different effects are involved within these zones of interest which includes pressure effect, temperature, and compaction effect. The gas charged sand reservoirs identified from the wells as velocities as follows: Vp_{mean}= 2,150 m/s, Vs_{mean}= 1,200 m/s

In a sonic log, the sonic velocity of gas-charged sand is lower than the sonic velocity of water-charged sand, while the sonic velocity of water charged sand is lower than the sonic velocity of surrounding shale. For example, the velocity of gas-charged sand in well #6 is 2,169 m/s, but the velocity of water-charged sand is 2,250 m/s, and the velocity of shale is 2,750 m/s. The gas in the sand reservoir reduces both the velocity and the density of the sand reservoirs.

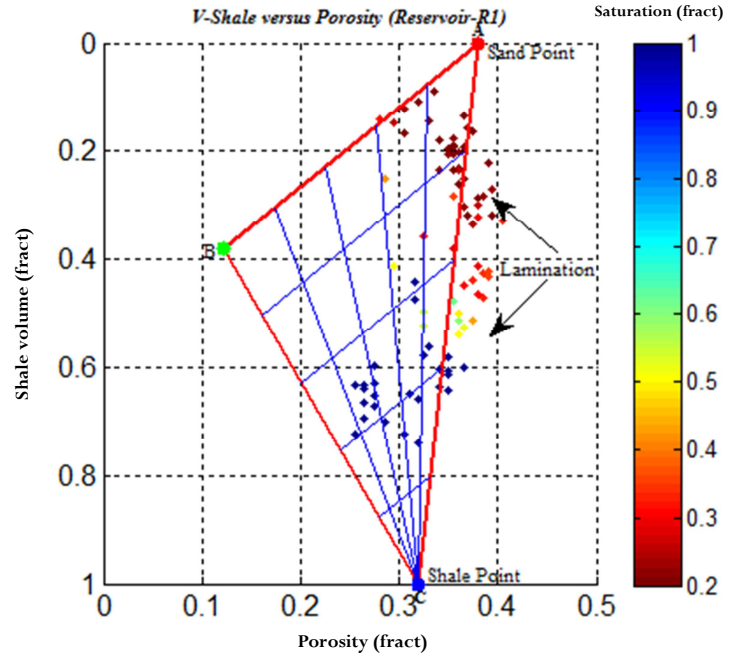

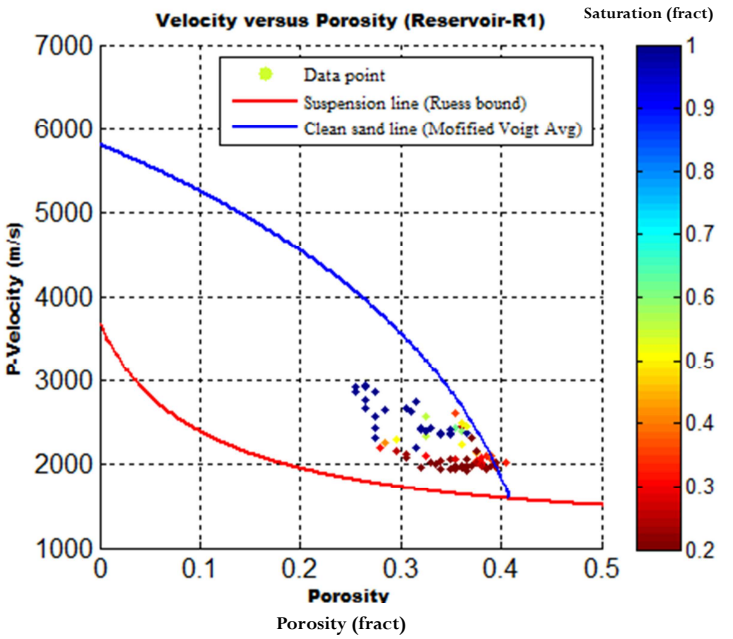

Figure 3.10a: Hybrid Thomas-Stieber-Dvorkin-Gutierrez model super-imposed on the data at reservoir (R1) from well 1 colour coded with water saturation

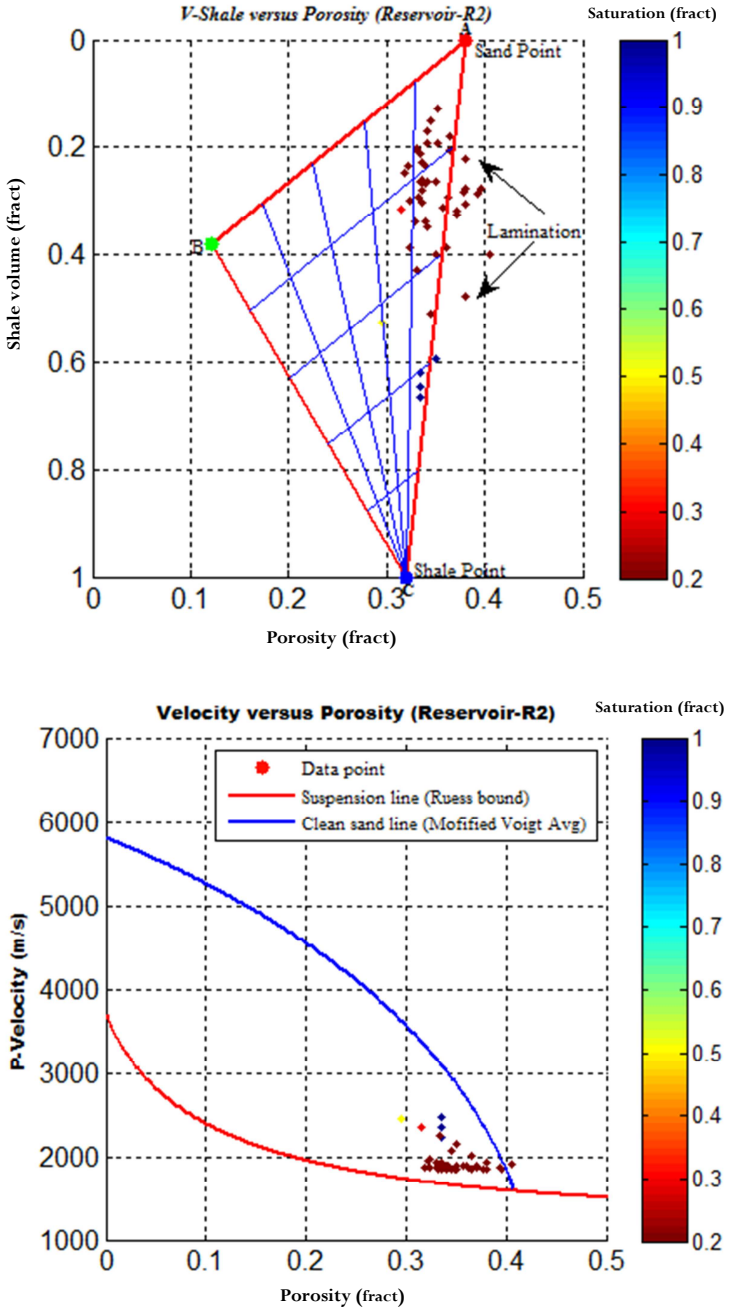

Figure 3.10b: Hybrid Thomas-Stieber-Dvorkin-Gutierrez model super-imposed on well data at reservoir (R2) from well 1; colour coded with water saturation

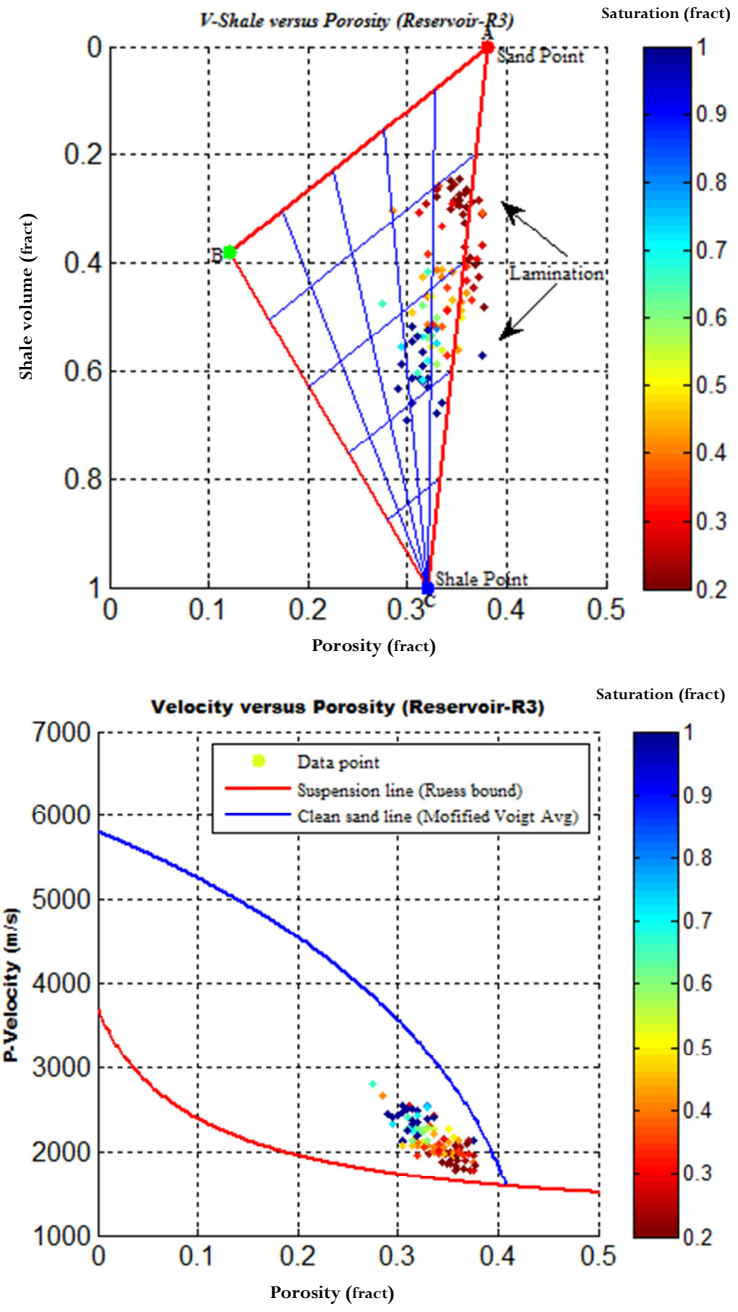

Figure 3.10c: Hybrid Thomas-Stieber-Dvorkin-Gutierrez model super-imposed on well data at reservoir (R3) from well 1; colour coded with water saturation

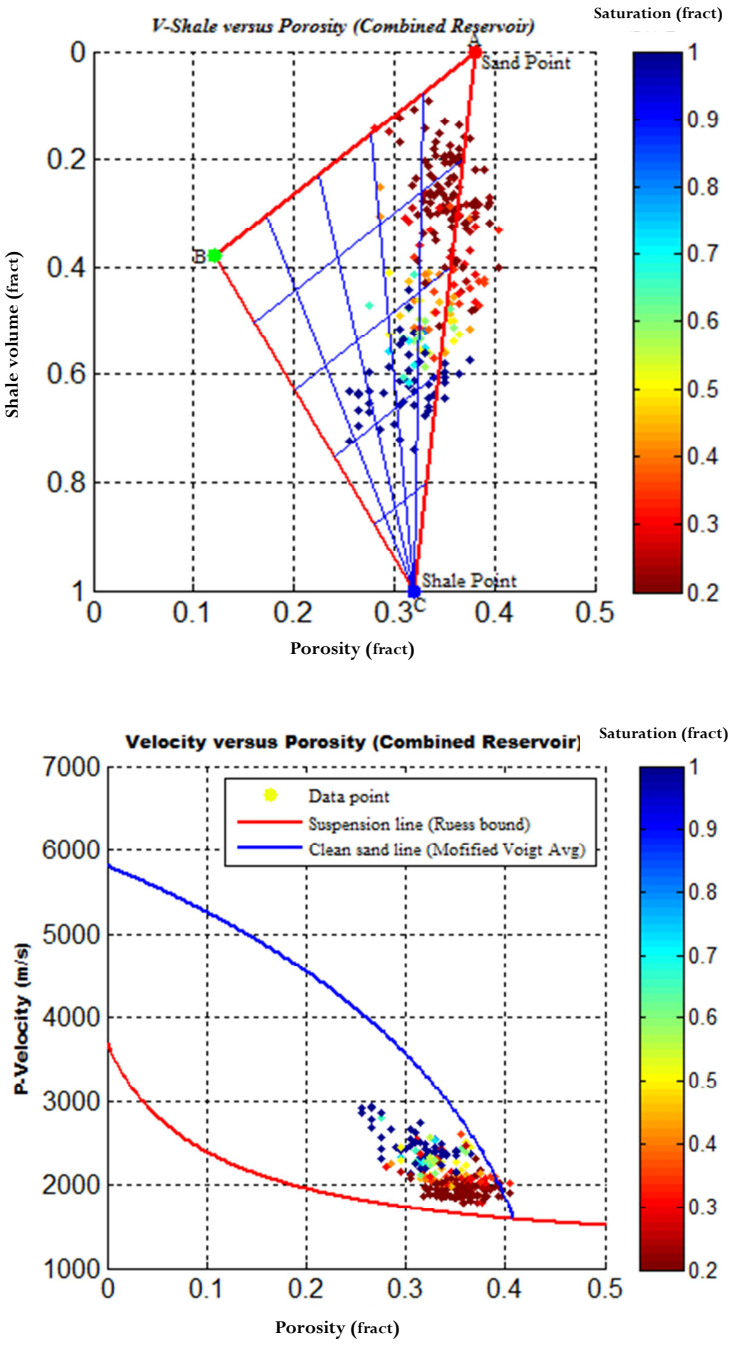

Figure 3.11: Hybrid Thomas-Stieber-Dvorkin-Gutierrez model super-imposed on the data for combined reservoirs from well 1; Colour coded with water saturation

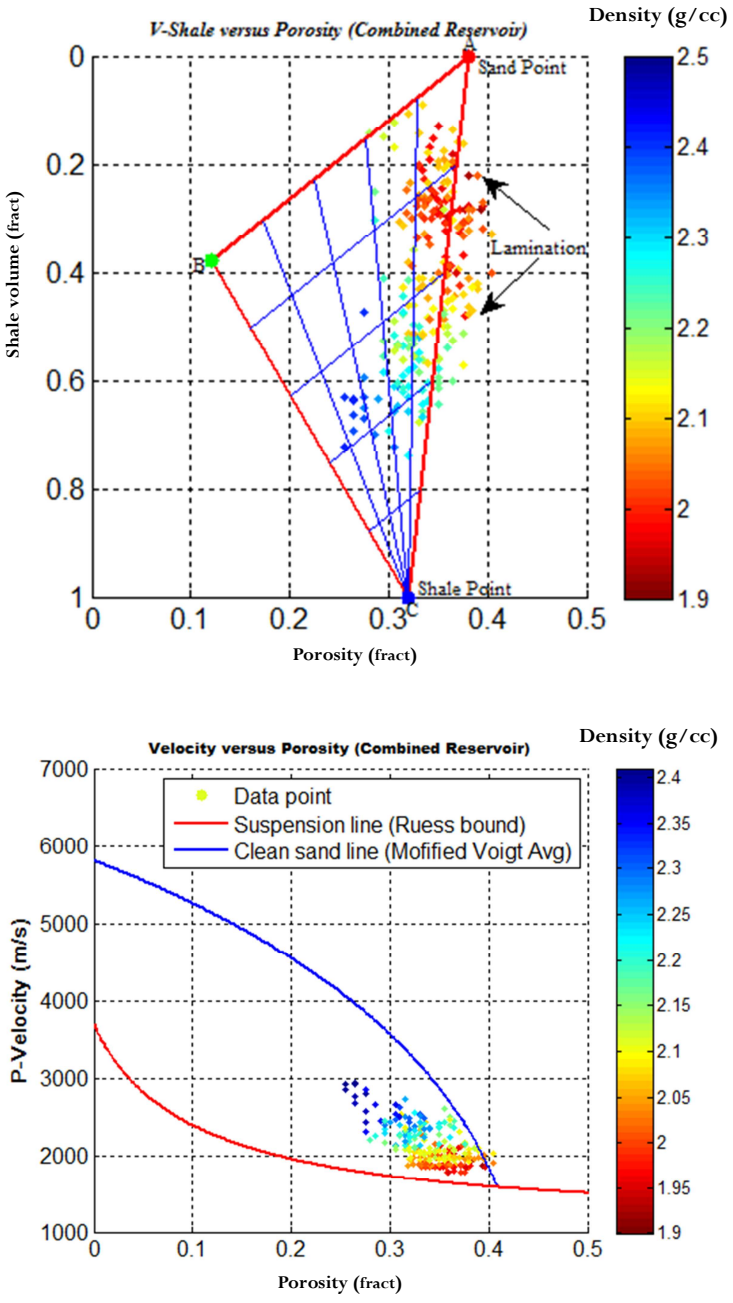

Figure 3.12: Hybrid Thomas-Stieber-Dvorkin-Gutierrez model super-imposed on the data for combined reservoirs from well 1; Colour coded with density

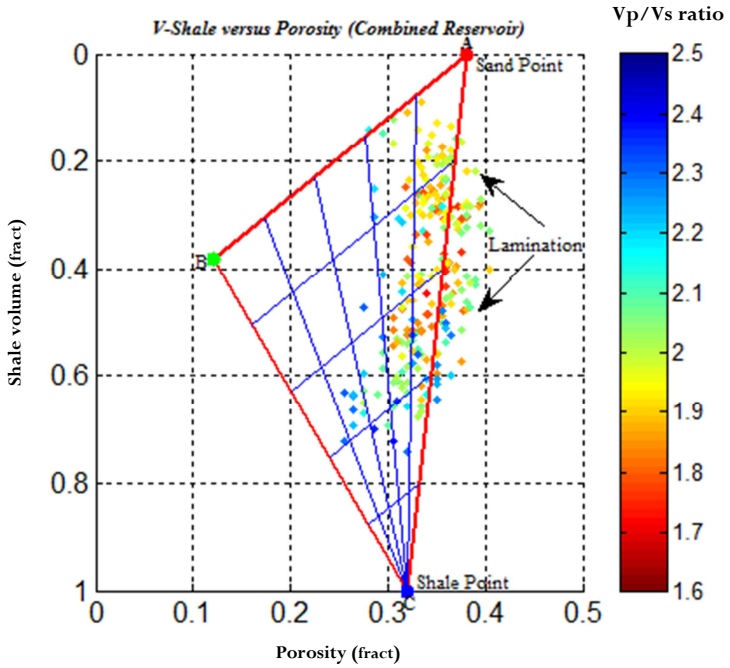

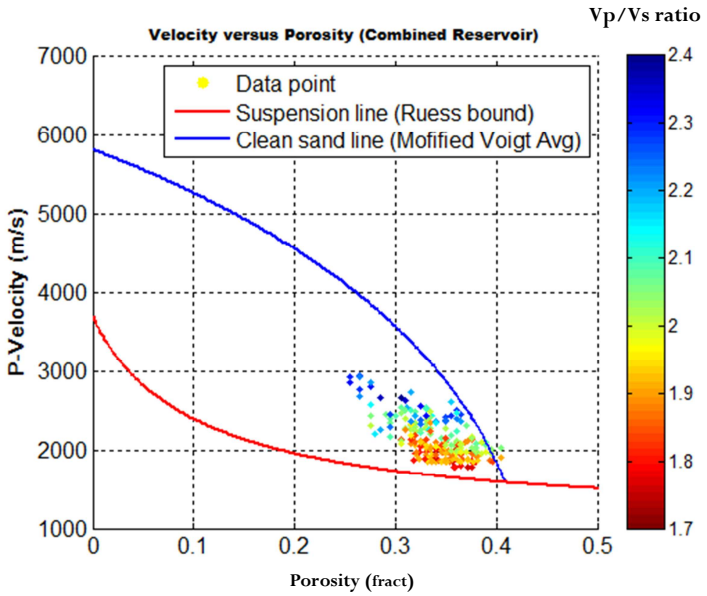

Figure 3.13: Hybrid Thomas-Stieber-Dvorkin-Gutierrez model super-imposed on the data for combined reservoirs from well 1; Colour coded with Vp/Vs ratio

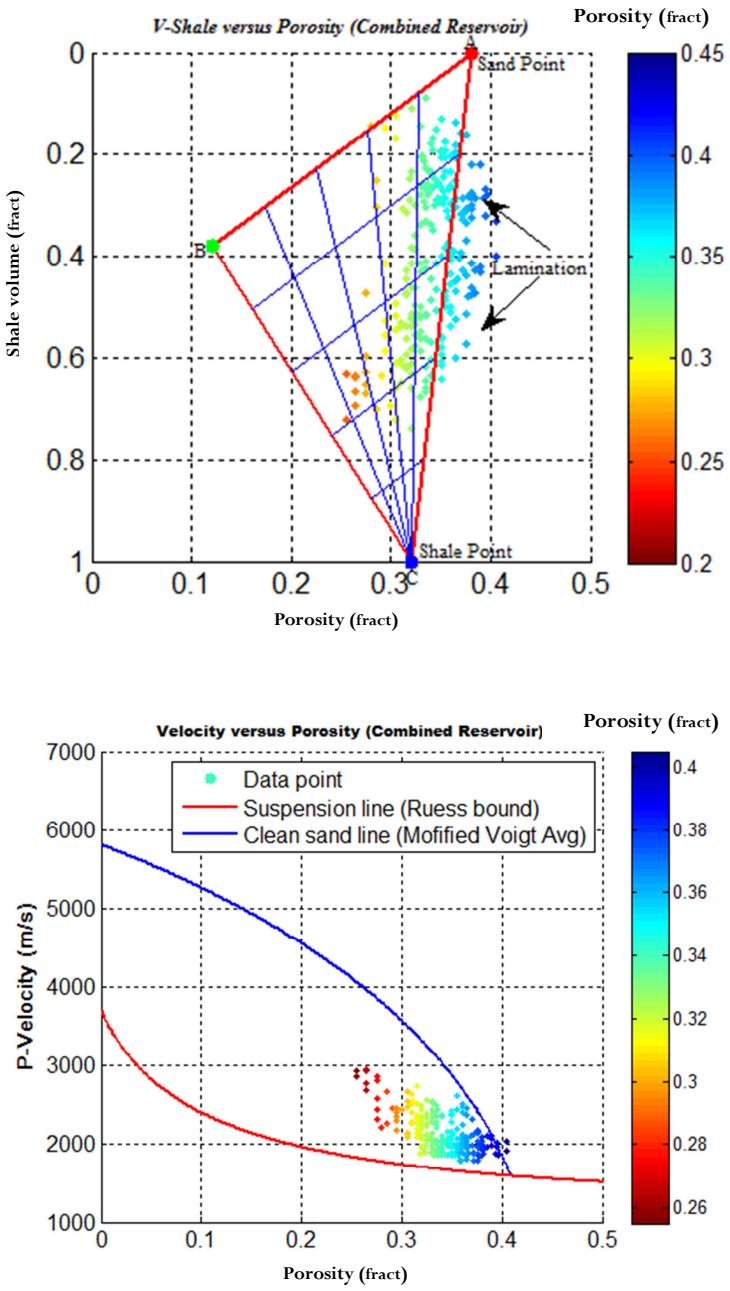

Figure 3.14: Hybrid Thomas-Stieber-Dvorkin-Gutierrez model super-imposed on the data for combined reservoirs from well 1; Colour coded with porosity

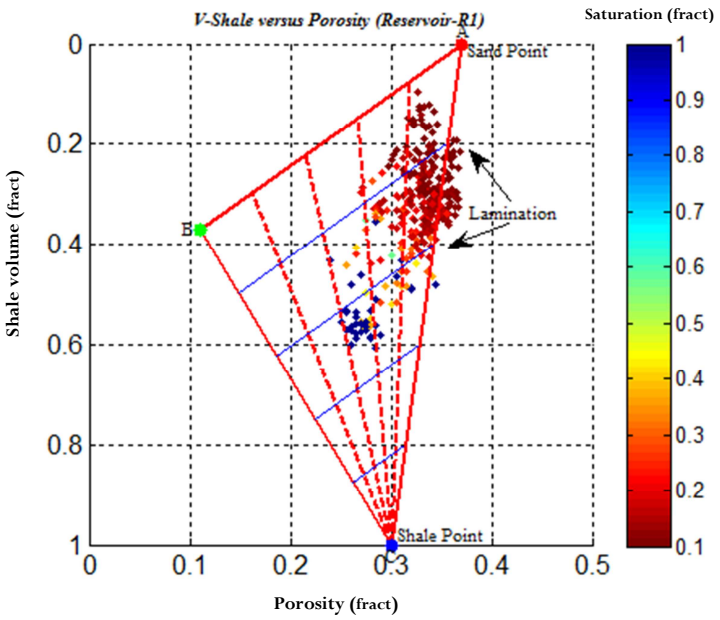

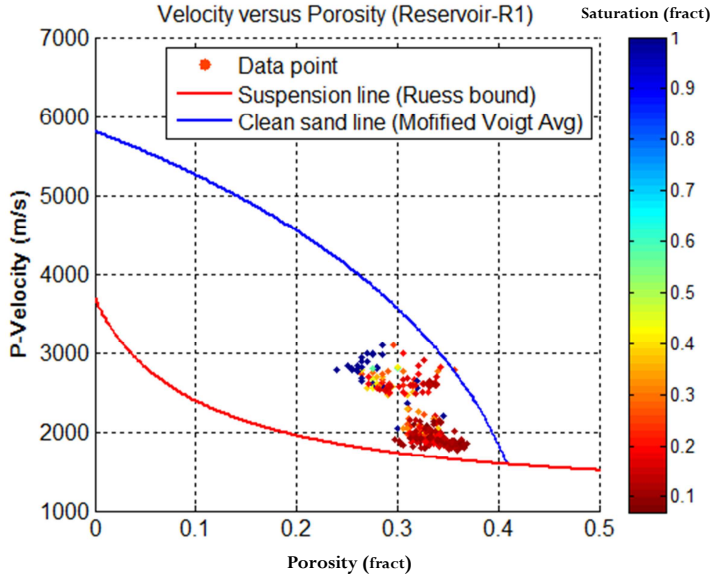

Figure 3.15a: Hybrid Thomas-Stieber-Dvorkin-Gutierrez model super-imposed on the data at reservoir (R1) from well 6 color coded with water saturation

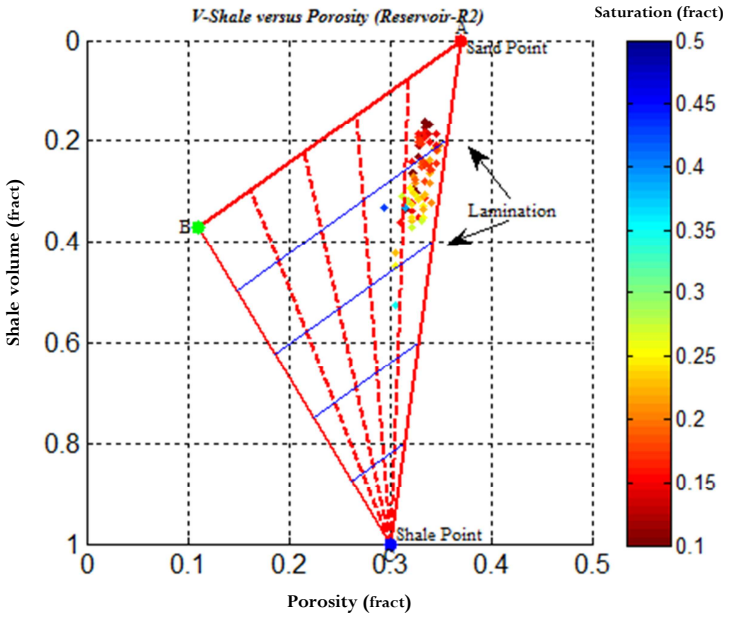

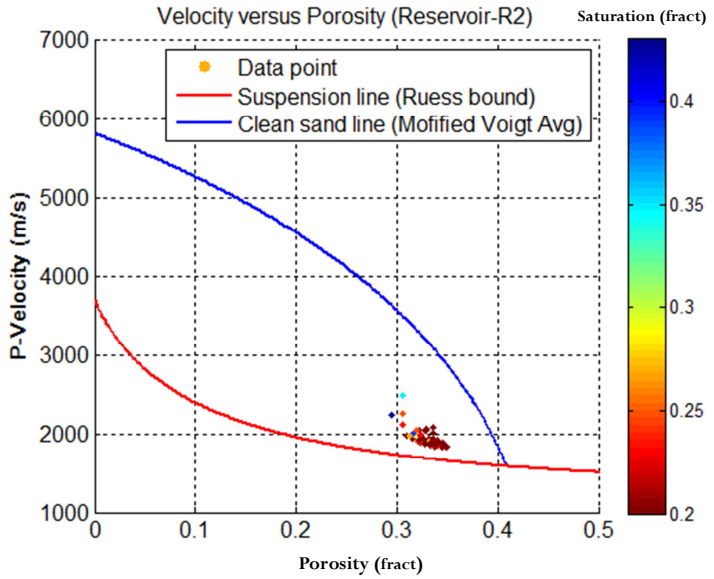

Figure 3.15b: Hybrid Thomas-Stieber-Dvorkin-Gutierrez model super-imposed on the data at reservoir (R2) from well 6 color coded with water saturation

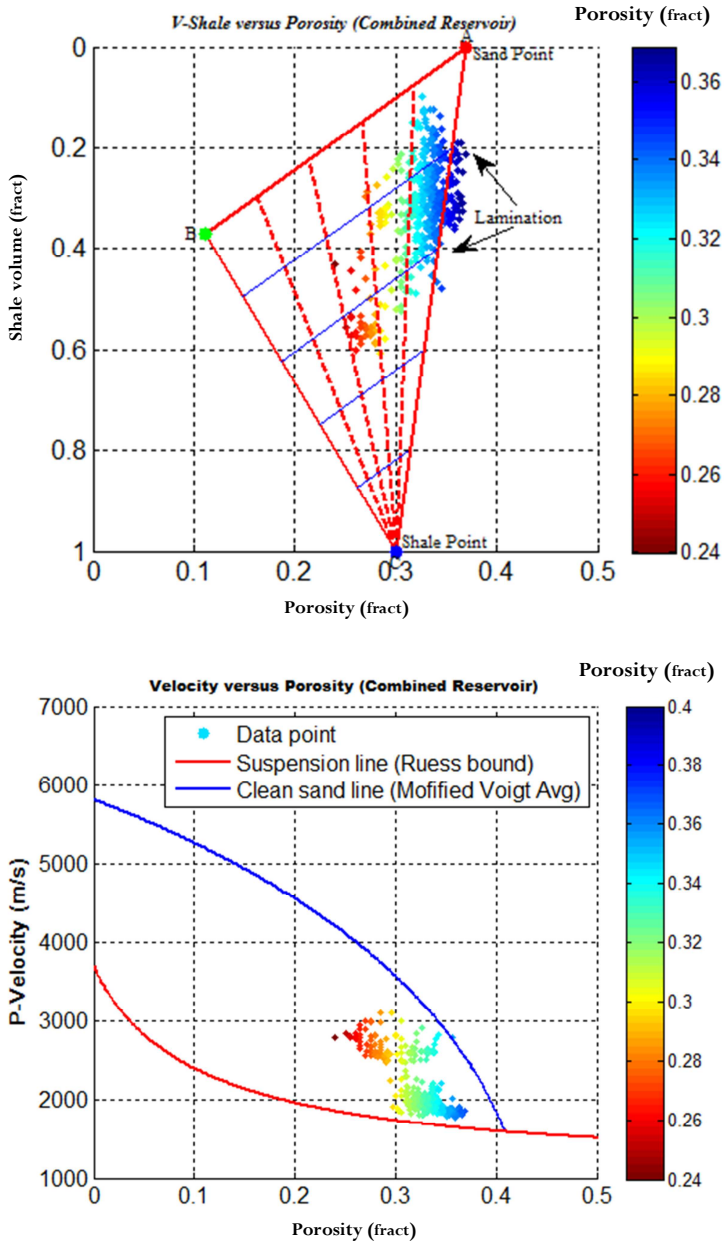

Figure 3.16: Hybrid Thomas-Stieber-Dvorkin-Gutierrez model super-imposed on the data for combined reservoirs from well 6; Colour coded with porosity

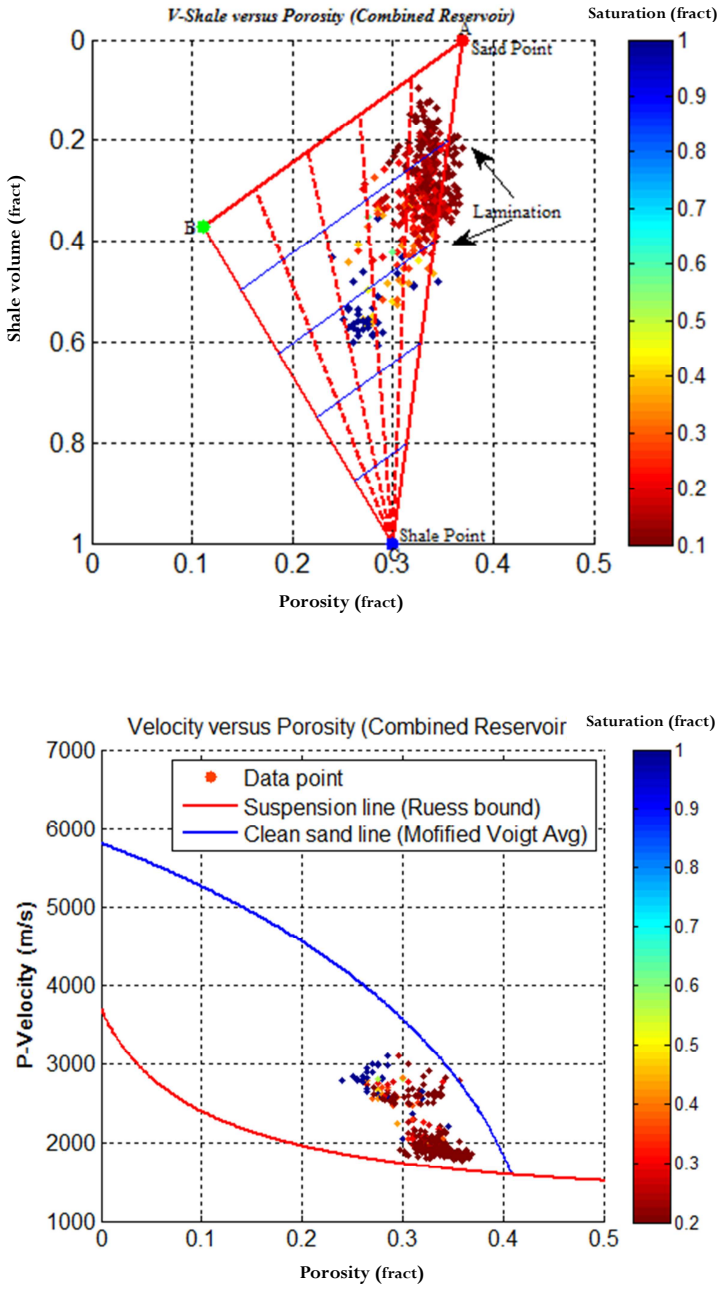

Figure 3.17: Hybrid Thomas-Stieber-Dvorkin-Gutierrez model superimposed on the data for combined reservoirs from well 6; Colour coded with water saturation

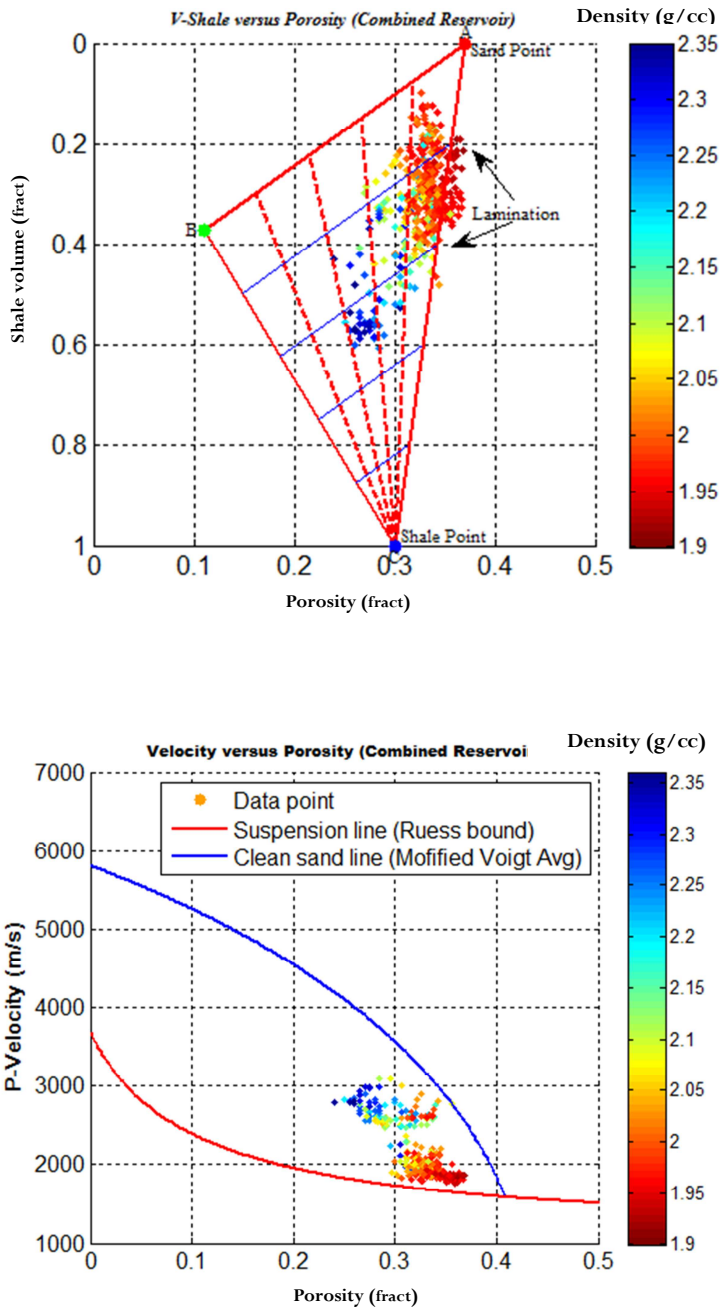

Figure 3.18: Hybrid Thomas-Stieber-Dvorkin-Gutierrez model super-imposed on the data for combined reservoirs from well 6; Colour coded with density

CHAPTER 4

FLUID REPLACEMENT MODELLING

5.2 Definition of Rock Composite (Sandstone-Shale System)

When considering a solid matrix composed of sandstones and shales sequence typical of a clastic environment, pores related to shales are assumed to be filled primarily by bound water (Figure 4.1). The total pore space is partitioned into clay-related pores and sandstone-related pores, and only sandstone-related pores are filled using Gassmann's theory (Figure 4.1).

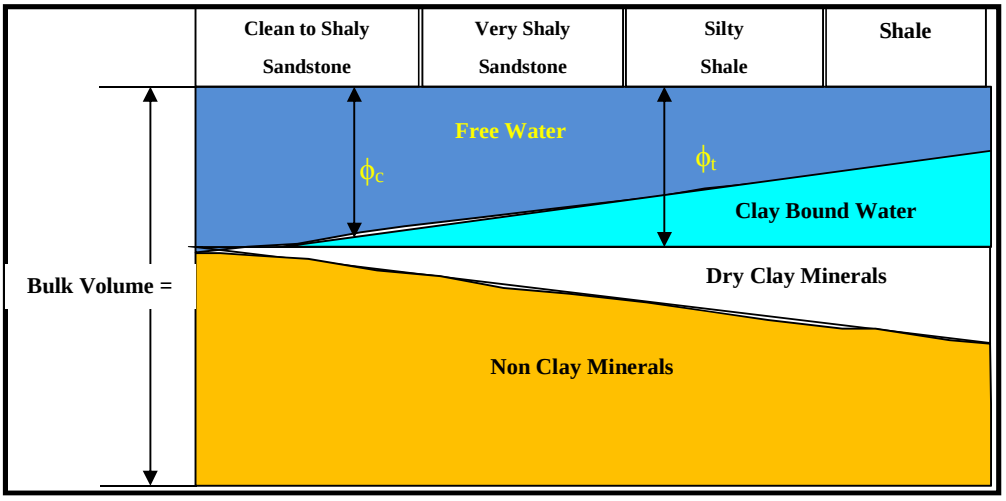

Figure 4.1: The sandstone-shale composite (After Truman, 1989)

The term shales is refer to a fine-grained, sedimentary rock composed mainly of clays (~60%) and other minerals, like quartz, feldspar, *etc.*, characterized by three attributes (Worthington, 2003):

(1) Clay minerals constitute the load-bearing framework;

(2) Shales have nanometer pore sizes and nanodarcy permeability;

(3) Surface area is large, and water is adsorbed on surfaces or bound inside clay platelets.

As seen from the above attributes, shale definition encompasses both grain size (<3.9 micrometers), and mineralogy (denoting illite, smectite, chlorite, kaolinite, and other hydrous phyllosilicates). These two meanings of clay overlap significantly in practice but are not identical.

5.3 Gassmman's Theory

Fluid substitution is a prediction of fluid saturation effects on seismic properties. This is an important part of the seismic rock physics analysis (e.g., AVO, 4D analysis), which provides a tool for fluid identification and quantification in reservoir (Nasser, 2012). This is commonly performed using Gassmann's equation (equation 22) to calculate elastic properties at the desired saturation, from either the dry rock or a rock saturated with another fluid (Gassmann, 1951; Sheriff, 2006). Gassmann's equation is the low frequency limit (relaxed fluid-rock state) for wave

propagation in saturated media. Figure 4.2 explains basic assumption taking while using Gassmann's equation.

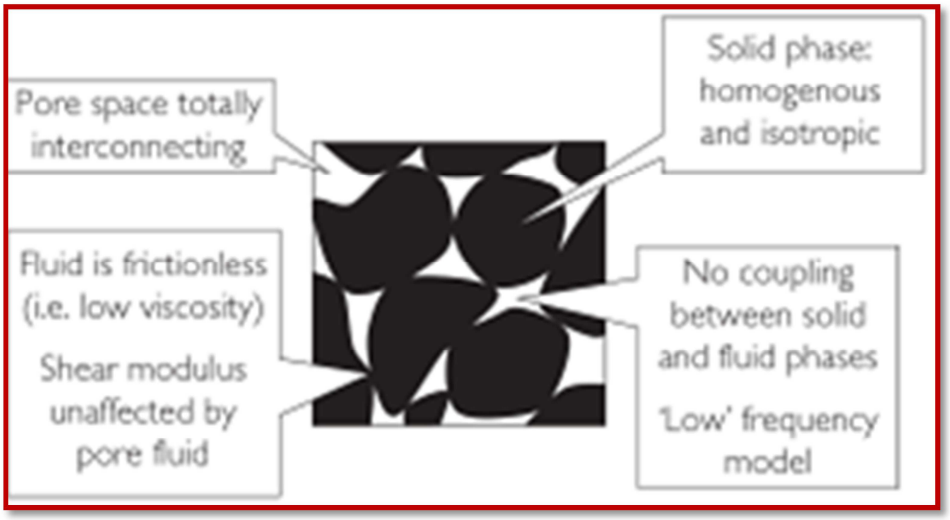

Figure 4.2: Schematic illustration of the key assumptions in Gassmann's equation (After Rob Simm and Mike Bacon, 2003)

The objective of fluid substitution is to model the seismic properties (seismic velocities) and density of a reservoir at a given reservoir condition (e.g., pressure, temperature, porosity, mineral type, and water salinity) and pore fluid saturation such as 100% water saturation or hydrocarbon with only oil or only gas saturation.

$$K_{sat} = K_{frame} + \frac{\left(1-\frac{K_{frame}}{K_{matrix}}\right)^2}{\frac{\emptyset}{K_{fl}}+\frac{(1-\emptyset)}{K_{matrix}}+\frac{K_{frame}}{K^2_{matrix}}} \qquad (22)$$

$$\mu_{sat} = \mu_{frame}$$

Where,

$K_{frame} =$ effective bulk modulus of dry rock;

$K_{sat} =$ effective bulk modulus of rock with pore fluid;

$K_{matrix} =$ effective bulk modulus of mineral material making the rock;

$K_{fluid} =$ effective bulk modulus of pore fluid;

$\mu_{frame} =$ effective shear modulus of dry rock;

$\mu_{sat} =$ effective shear modulus of rock with pore fluid;

$\emptyset = Porosity$

The density and bulk modulus of water are functions of temperature, pressure, and salinity. The properties of hydrocarbons, oil, and gas, are more variable and depend strongly on temperature, pressure, and composition (Murphy, 1993).

Fluid density (ρfl) is a mixture of fluids weighted by saturation - the amount of pore space filled with particular fluid type, and it is defined using equation:

$$\rho_{fl} = S_w\rho_w + (1 - S_w)\rho_{hc}\,, \qquad (23)$$

Where,

$S_w =$ water saturation in decimal fraction;

$\rho_w =$ density of formation water;

$\rho_{hc} =$ density of hydrocarbon.

The fluid modulus is given by Wood's equation:

$$K_{fl} = \left(\frac{S_w}{K_w} + \frac{(1-S_w)}{K_{hc}}\right)^{-1}, \qquad (24)$$

Where,

$K_w \; and \; K_{hc} =$ bulk modulus of brine and hydrocarbon, respectively;

$S_w =$ water saturation in decimal fraction;

The mass balance equation is used to calculate the bulk density of the rock as a function of porosity and mixed fluids:

$$\rho_b = \rho_g(1 - \phi) + \rho_{fl}\phi\,, \tag{25}$$

Where,

$\rho_b =$ $bulk$ density of the formation;

$\rho_g =$ density of the grains comprising the formation (sand grain density 2.65 g /cc);

$\rho_{fl} =$ density of fluid;

$\emptyset = Porosity$.

The compressional (Vp) and shear velocity (Vs) are calculated for the new/desired saturation using the following equations:

$$V_p = \sqrt{\frac{K_{sat}+4/3\,\mu}{\rho_b}} \tag{26}$$

$$V_s = \sqrt{\frac{\mu}{\rho_b}} \tag{27}$$

Gassmann's theory includes several assumptions (Wang, 2001). The rock is macroscopically homogeneous and monomineralic. All the pores are communicating (pressure is able to equilibrate, which relates to zero frequency assumption). The pores are filled with frictionless fluid (the viscosity of the saturating fluid is zero).

The rock-fluid system is closed (undrained). There is no interaction between solid and fluid (no hardening or softening the frame due to interactions with fluid).

5.4 Fluid Substitution on Geophysical Logs

From geophysical logs, fluid substitution is performed using Gassmann's equation. Most of the necessary information for fluid substitution using Gassmann's equation can be derived from geophysical logs. The input logs are resistivity, neutron porosity, bulk density, P-wave velocity, and S-wave velocity. The practicality of using Gassmann's equation is well spelt out in figure 4.3 as it relate to geophysical logs.

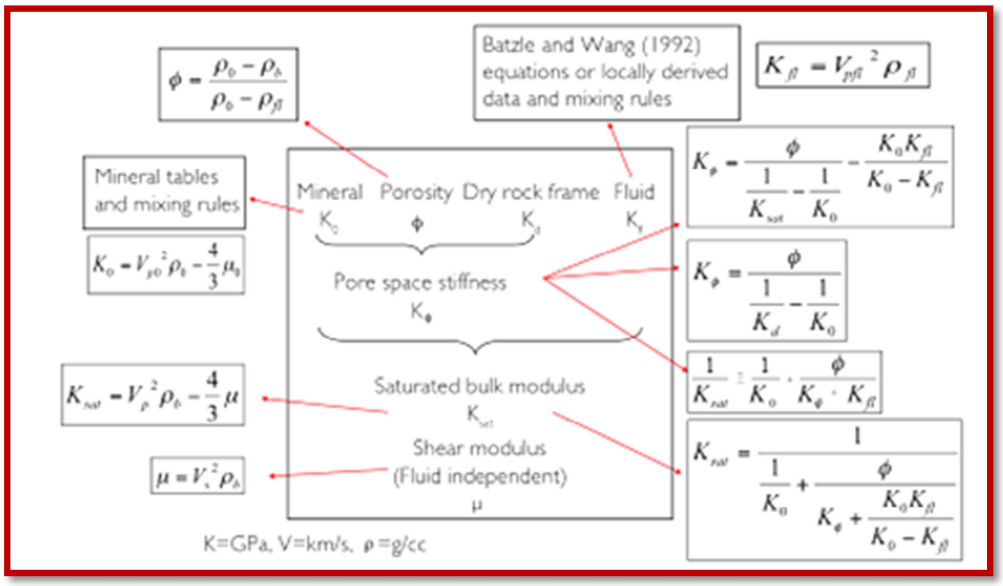

Figure 4.3: Practical equations for the application of Gassmann's relations to log data (After Rob Simm and Mike Bacon, 2003)

Inverting Rock Frame Properties Using Gassmann Fluid Substitution:

To invert properties for dry rock moduli, the Gassmann equation is used through the following procedure (modified after Smith *et al*., 2003):

1. Log edits and interpretation.

2. S-wave velocity estimation (if necessary).

3. Calculate bulk and shear moduli for *in situ* conditions using the following equation:

$$K_{sat} = \rho_b \left(V_p^2 - \frac{4}{3} V_s^2 \right) \quad (28)$$

$$\mu_{sat} = \rho_b V_s^2 , \quad (29)$$

Where ρ_b , V_p , V_s are density and velocities (sonic travel time) as logged, without any correction applied.

4. Calculate K_o based on lithology estimates (volume of shale). Magnolia lithology is siliciclastic sandstones, shales, and mixture of the two. So, we assume that the formation is comprised of quartz minerals and shales, that it is homogeneous and isotropic in macro sense.

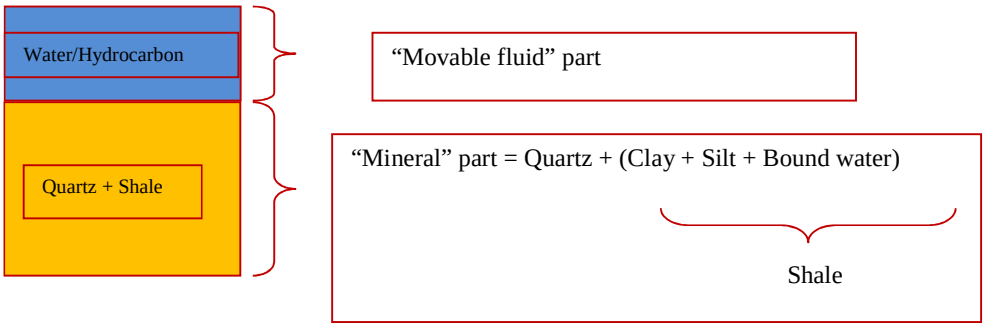

Figure 4.4: The sandstone-shale system as modelled (After Milovac, 2009).

We assume that shale above, below, and within the reservoir is the same, and that the difference between total and effective porosity is due to clay-bounded water.

We assume the bulk modulus for quartz is 37 GPa, and the shear modulus for quartz is 40 GPa. Shale properties have been extracted from the logs in a zone with the highest shale fraction (volume of shale equal to 100%). Bulk modulus for shale is 14 GPa, shear modulus for shales is 2.7 GPa. Then we mixed quartz and shale using the Hill average (Mavko *et al*., 1998):

$$K_{Reuss} = \left[\frac{V_{clay}}{K_{clay}} + \frac{V_{qtz}}{K_{qtz}}\right]^{-1} \quad (30)$$

$$K_{Voigt} = \left(V_{clay}K_{clay} + V_{qtz}K_{qtz}\right) \quad (31)$$

$$K_{vrh} = \frac{1}{2}\left(K_{Voigt} + K_{Reuss}\right) \quad (32)$$

Where,

V_{clay} and V_{qtz} = volume fractions of sands and shales;

$K_{clay}\ and\ K_{qtz}$ = shale and quartz bulk moduli.

Or

$$K_{matrix} = \frac{1}{2}\left(\left[V_{clay}K_{clay} + V_{qtz}K_{qtz}\right] + \left[\frac{V_{clay}}{K_{clay}} + \frac{V_{qtz}}{K_{qtz}}\right]\right)$$

Where *Vclay* and *Vqtz* are

$$V_{clay} = 70\%V_{sh}\ (this\ is\ an\ assumption)$$

and

$V_{qtz} = 1 - V_{clay}$,

5. Calculate fluid properties. Fluid properties estimation has been described in the previous section. The same properties have been used here.

6. Mix fluid densities and moduli for *in situ* case according to Sw.

7. Calculate K_{frame}. "The 'frame' frame modulus refers to the incremental bulk deformation resulting from an increment of applied confining pressure with pore pressure held constant" (Mavko *et al.*, 2009). It is a function of porosity, mineral modulus, fluid modulus and modulus of a saturated rock, and is given by:

$$K_{frame} = \frac{K_{sat}\left(\frac{\emptyset K_{matrix}}{K_{fl}} + 1 - \emptyset\right) - K_{matrix}}{\frac{\emptyset K_{matrix}}{K_{fl}} + \frac{K_{sat}}{K_{matrix}} - 1 - \emptyset} \qquad (33)$$

8. Calculate the "dry" bulk density (density of fluid equal to zero).

9. Calculate the "dry" compressional and shear velocity.

5.5 Fluid Substitution In Laminated Sandstone-Shale Sequence

Fluid replacement modelling using Gassmann's equation in thinly bedded sandstone–shale sequences was presented by Dejtrakulwong and Mavko (2011). Dejtrakulwong *et al.* 2011 proposed a new method for doing this using the Thomas-Stieber (1975) model to detect laminations and then downscale for the sand and shale end-members' properties, apply Gassmann's equation to sandstone layers only, and then upscale the layers back using the Bakcus average (Nasser *et al.* 2013). Nasser *et al*. 2013 proposed a fluid substitution in laminated sandstone and shale using a two-step process steps requiring shale delamination to accurately compute dry and

saturated bulk moduli for the sand only, and then mix the delaminated shale and the saturated sandstone using the Reuss average (figure 4.5).

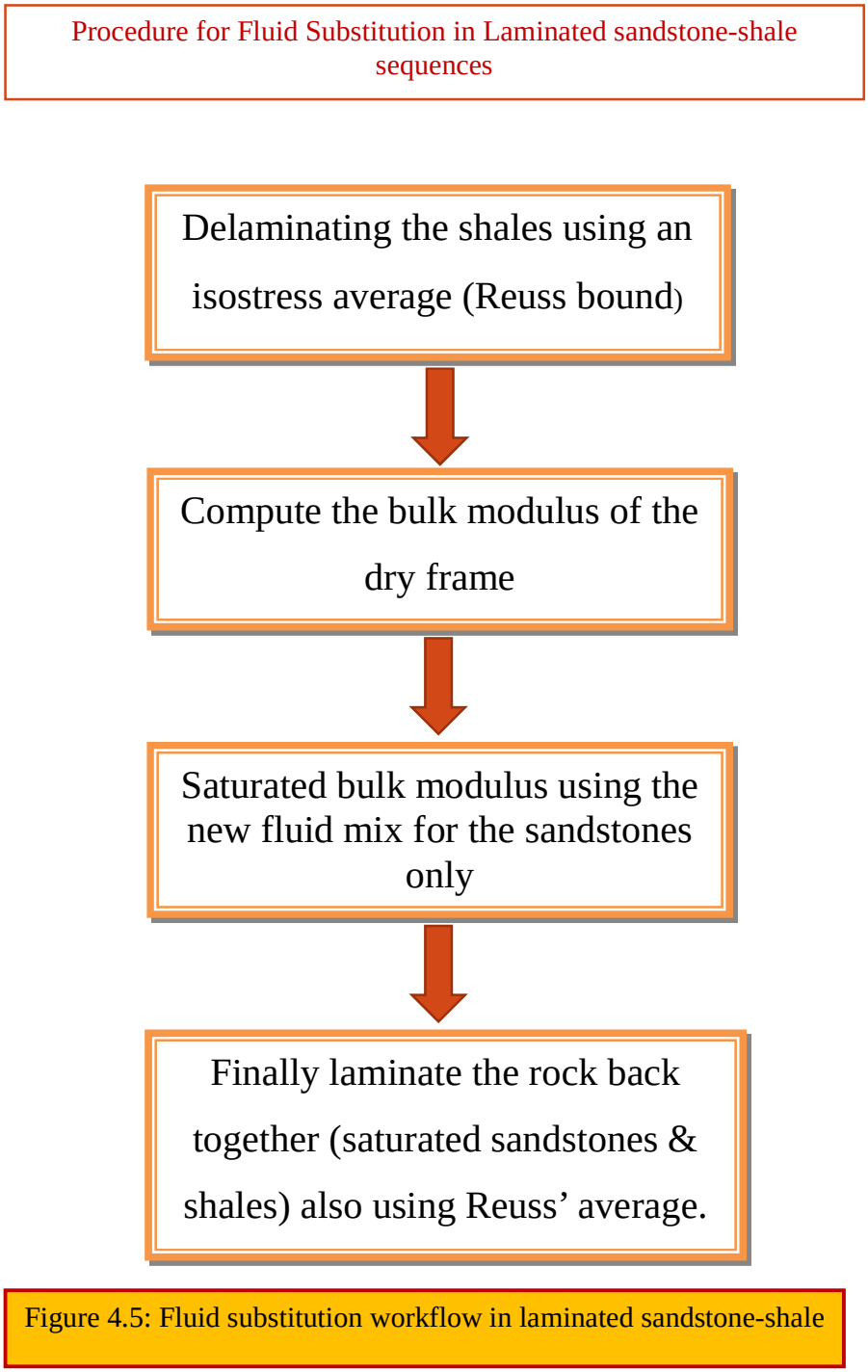

Figure 4.5: Fluid substitution workflow in laminated sandstone-shale

Steps for delamination and fluid substitution in sandstone - shale sequence (Nasser *et. al.* 2013)

1. Define your Bulk moduls (K), shear modulus (μ) and density (rho) for solid matrix i.e. K=37 GPa, μ=45 GPa and rho=2.650
2. Derive shale trends as a function of depth (Vp, Vs and rho)
3. From step 2, calculate K and μ for shale (data from well log)

$$K_{shale} = rho * V_p^2 - {}^4/_3 * rho * V_s^2 \quad (34)$$

$$\mu_{shale} = V_s^2 * rho \quad (35)$$

4. Read your log Vp, Vs and rho
5. From step 4 calculate K and μ
6. Calculate your in-situ fluid bulk modulus and density

$$K_{fluid} = \left[\frac{S_{w1}}{K_{w1}} + \frac{(1 - S_{w1})}{K_{h1}}\right]^{-1}$$

$$\rho_{fluid} = S_{w1} * \rho_{w1} + (1 - S_{w1}) * \rho_{h1}$$

Kh1= Bulk modulus of hydrocarbon in the original fluid (GPa)

ρh1= Density of hydrocarbon in the original fluid (g/cc)

Kw1= Bulk modulus of brine in the original fluid (GPa)

ρw1= Density of brine in the original fluid (g/cc)

Sw1= Brine saturation of rock in the original fluid (fraction)

7. For the delaminating stage:

Gassmann account for the combined volume and distribution of shale i.e., disperse, laminated and structural shale.

$$Volume_{Shale} = Volume_{disperse} + Volume_{laminated} + Volume_{structural}$$

Where Volume of sand (V_{sand} =1-V_{sh})

From effective medium theory;

$$\frac{1}{K_{sat\,1}} = \frac{V_{sh}}{K_{shale}} + \frac{1 - V_{sh}}{K_{sand}}$$

$$\frac{V_{sand}}{K_{sand}} = \frac{1}{K_{sat\,1}} - \frac{V_{sh}}{K_{shale}}$$

$$Multiply\ both\ sides\ by\ \frac{1}{V_{sand}}$$

$$\frac{V_{sand}}{K_{sand}} * \frac{1}{V_{sand}} = \frac{1}{K_{sat\,1}} * \frac{1}{V_{sand}} - \frac{V_{sh}}{K_{shale}} * \frac{1}{V_{sand}}$$

$$\frac{1}{K_{sand}} = \frac{\frac{1}{K_{sat\,1}} - \frac{V_{shale}}{K_{shale}}}{V_{sand}}$$

$$K_{sand} = \frac{V_{sand}}{\frac{1}{K_{Sat\,1}} - \frac{V_{shale}}{K_{shale}}}$$

$$K_{sand} = \frac{1 - V_{shale}}{\frac{1}{K_{Sat\,1}} - \frac{V_{shale}}{K_{shale}}} \qquad (36)$$

8. Compute Dry bulk or frame modulus

$$a = \frac{K_{sand\,1}}{K_{quartz} - K_{sand\,1}}$$

$$b = \frac{K_{fluid\,1}}{(Phi_{sand} * (K_{quartz} - K_{fluid\,1}))}$$

$$K_{dry} = K_{quartz} * \frac{(a-b)}{(1+a-b)} \quad (37)$$

9. Use K_{dry} from equation 8 to compute K_{sand2}

$$K_{sat2} = K_{frame} + \frac{\left(1 - \frac{K_{frame}}{K_{matrix}}\right)^2}{\frac{\emptyset}{K_{fl}} + \frac{(1-\emptyset)}{K_{matrix}} + \frac{K_{frame}}{K_{matrix}^2}} \quad (38)$$

$\varphi = \varphi_{sand}$ and $K_{matrix} = K_{quartz} = 36.5$

10. Use φ_sand, K_quartz

11. We have computed K_sat 2 (For sand)

12. Laminate back the shales and sands using Reuss aveage

$$K_{sat\ 2} = \frac{1.0}{\frac{V_{shale}}{K_{Shale}} - \frac{1-V_{shale}}{K_{sand}}} \quad (39)$$

13. Compute density, Vp and Vs using

$$rho_{sat2} = rho_{sat\ 1} - \varphi * (1 - V_{shale}) * \left(rho_{fluid} 1 - rho\ fluid\ 2\right)$$

$$V_{p_{sat\_2}} = \sqrt{\frac{K_{sat\_2} + \frac{4}{3}\mu\_sat\_2}{\rho_{b\_sat\_2}}} \quad (40)$$

$$V_{s\_sat\_2} = \sqrt{\frac{\mu\_sat\_2}{\rho_b\_sat\_2}} \quad (41)$$

5.6 Results and Discussion

The reservoir sandstones delineated in Magnolia field were investigated for effect of fluid changes within the reservoirs. Fluid substitution modelling was carried out on the hydrocarbon saturated reservoir sandstones using the Gassmann's equation and the Batzle and Wang equation (Batzle and Wang, 1992). The bulk modulus in the shale zones reaches about 14 GPa, this is the extracted value from moduli from log data in a shaliest interval in the section. In the sandstone zone, it ranges from 2.5 – 4.5 GPa. It shows that shale content often time reduces the moduli in sandstone, and such causes decreasing velocities. From all the parameters in Gassmann's equation, K_{dry} is probably the most difficult to estimate. It usually accumulates errors that were propagated through all the computation which includes incorrect matrix properties, incorrect fluid properties, incorrect initial porosities and saturation, presence of shale/clay etc. The elastic moduli of clay are much smaller compare to those of quartz, feldspar, calcite, and dolomite. Thus, large amounts of clay mineral can cause the average mineral method to incur errors. Elastic properties of clay minerals are not well known although some clay properties measurements have been published (Wang *et al.* 2001), and are often widely different. Figure 4.6 shows the fluid substitution results in well one, it is observed that P-wave velocity, bulk density and the P – impedance increases with brine saturation. P-wave velocity increases between 5 – 7 %, bulk density increases with about 4 – 6 % and the P-impedance increases with about 10 – 12%. Figure 4.7 is the cross-plot of Vp/Vs ratio versus P-impedance at in-situ condition, the cross-plot is colour coded with various attributes such as saturation, porosity and shale volume. The attributes aided both fluid and lithology differentiation. The data points enclosed within the broken line corresponds with the

reservoir intervals picked at well location. The reservoir zones has low Vp/Vs ratio, low density, good or high porosity and less shaliness. The zone was interpreted as hydrocarbon- bearing intervals as it clearly shown in its fluid response. Figure 4.9 presents the summary of the fluid replacement exercise, in the interest zone; the in-situ fluid was identified as gas and water with an approximate water saturation of about 20%. While conducting the fluid replacement modelling, the gas reservoirs are replaced with 100% brine. It is noticed that we have an increase in density, P-wave velocity and P-impedance while we observed a slight drop in the shear velocity for all the reservoir zones. The overall effect of this leads to an increased P-impedance and Vp/Vs ratio. Further modelling as shown in figure 4.8 confirmed that the in-situ reservoirs are gas because of the observed similar response between in-situ condition and gas replaced scenario. However, the gas effect was not observed on the brine response. Figure 5 and figure 10 shows the work flow and output of fluid replacement modelling for De-laminated sandstone-shale sequence, the cross-plots of VpVs ratio versus P-impedance color coded with water saturation at well . The result has demonstrated that when thin laminations are not accounted for, the fluid substitution results are over-predicted and hence small sandstone fractions will show a fluid response at least twice as much as large sandstone fractions, which is incorrect.

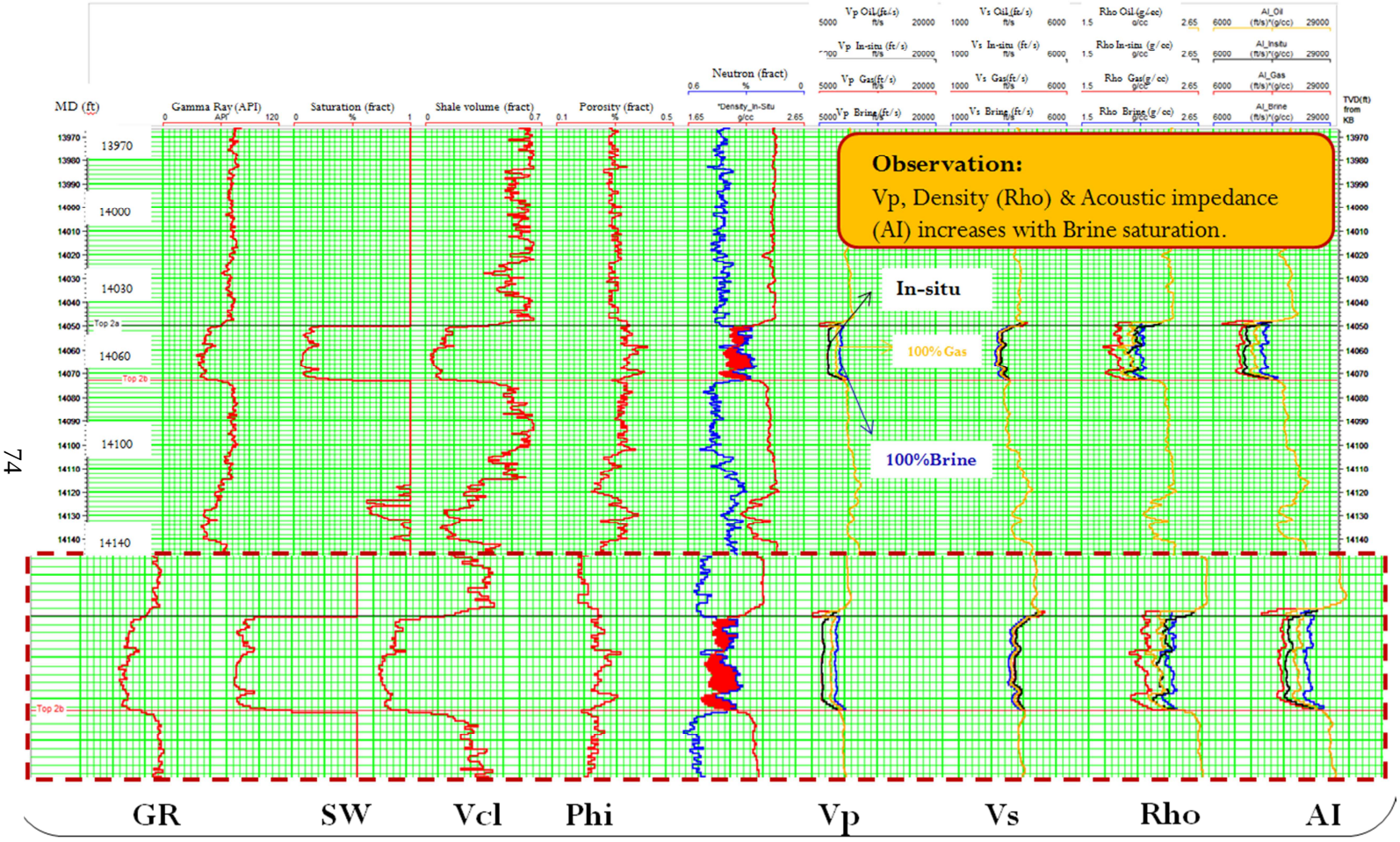

Figure 4.6: Fluid substitution result showing one of the reservoirs in well one

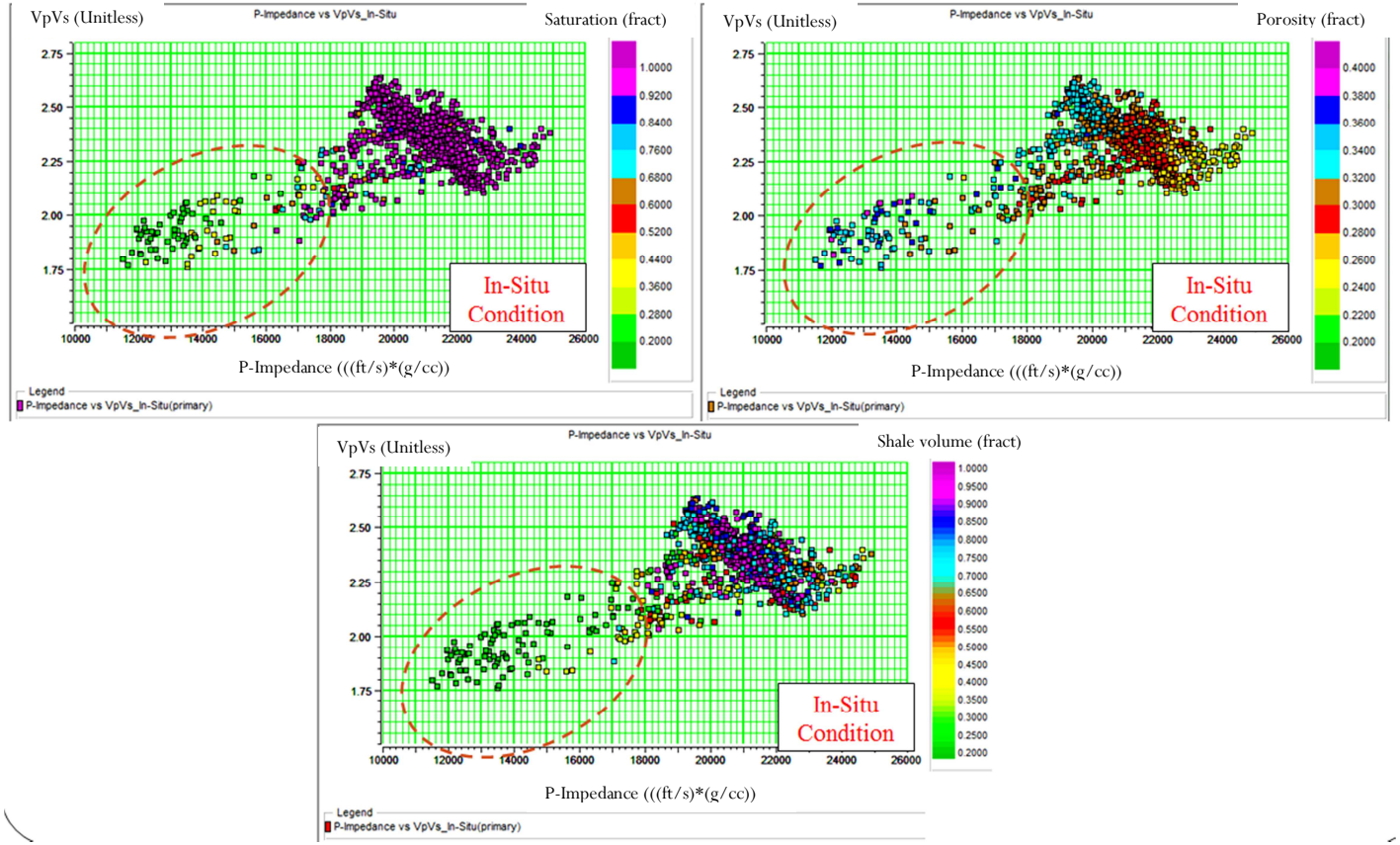

Figure 4.7: In-Situ condition Cross-plots of VpVs vs P-impedance; Colour coded with water saturation, porosity and volume of Shale at well 1

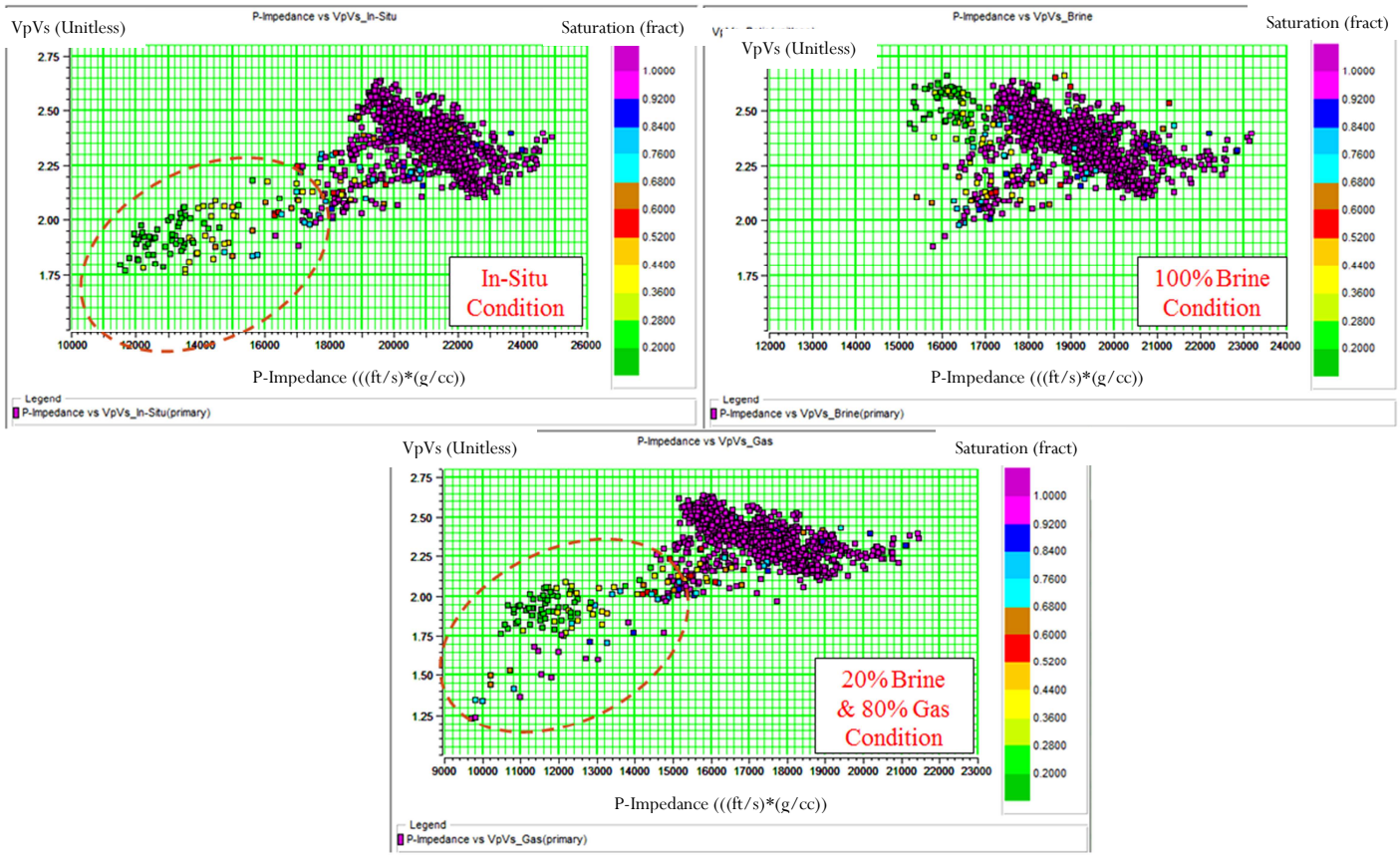

Figure 4.8: Fluid replacement modelling showing Cross-plots of VpVs vs P-impedance; Colour coded with water saturation at well 1

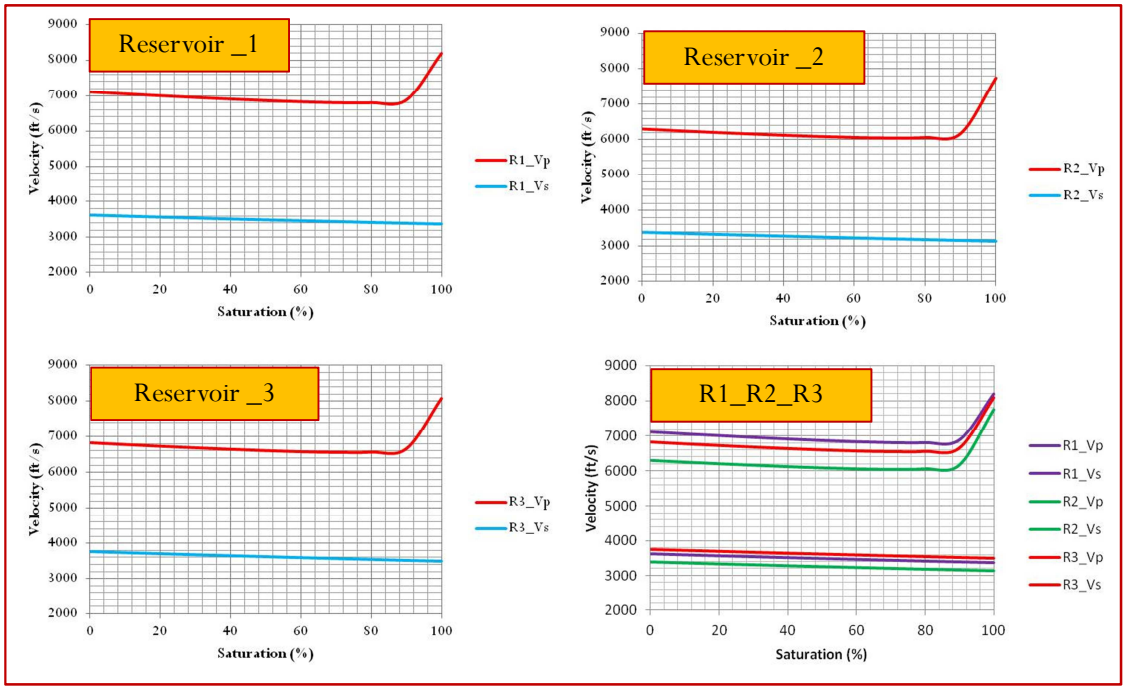

Figure 4.9: Crossplot of velocity versus fluid saturations at well 1; P-wave velocity drops from 0 to 20% gas saturation and to Increase from 30% gas saturation.

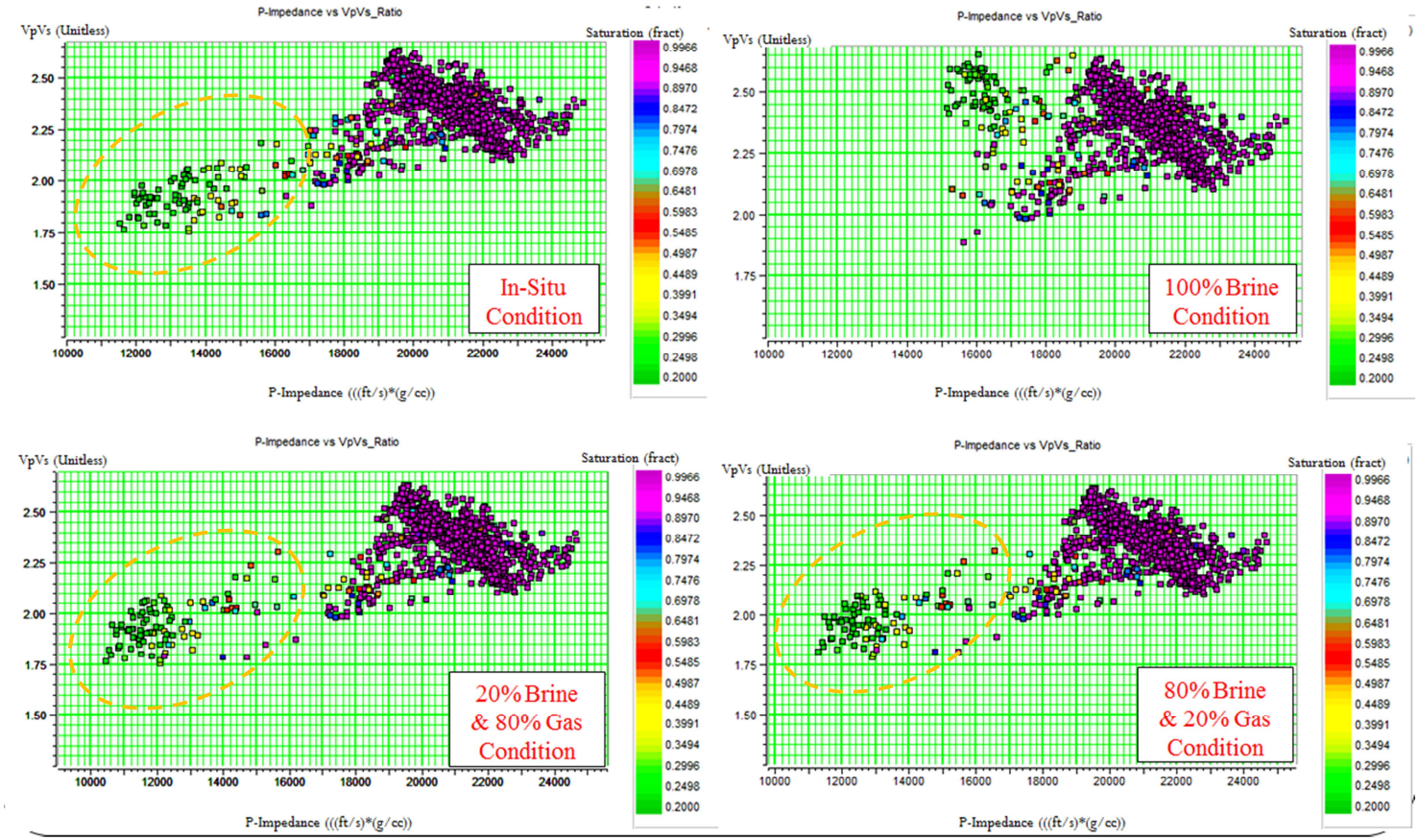

Figure 4.10: Fluid replacement modelling for De-laminated sand- shale sequence showing Cross-plots of VpVs vs P-impedance; Colour coded with water saturation at well 1

CHAPTER 5

CONCLUSION

5.1 Conclusion

- Petrophysics and rock physics approach was used to investigate and texturally interpret well log data from deep-water Magnolia field, offshore Louisiana.
- The Thomas–Stieber model was able to predict and describe the porosity-shale volume relations resulting from various mode of sandstone–shale mixing.
- The Dvorkin and Gutierrez model predicts the associated P-wave velocities. The combination of the Thomas-Stieber and Dvorkin-Gutierrez models gives a greater degree of confidence while evaluating formation properties. The combined models from T-S-D-G are most applicable in unconsolidated or poorly consolidated sediments where porosity and elastic properties are dominated by laminar and dispersed mixing modes of sandstone and shale sequence.
- From the above approach, dominant clay distribution pattern observed in the reservoirs delineated in Magnolia field are laminated clay. Dispersed and structural clays are rarely observed within the field. Consequent to this observation, it is concluded that this distribution pattern of clay heterogeneity has less significant effects on the petrophysical parameters considered.
- Reservoirs with laminated clays affect the net-to-gross ratio the most. Porosity values are seldom affected by lamina clays when shale volume is minimal. Clay laminas within reservoir serve as vertical permeability barrier; hence horizontal movement of hydrocarbons will be favoured during production.

- Because the reservoirs observed in the field are not complicated, Gassmann's fluid substitution (water, oil and gas) approach was able to handle various fluid scenarios. In situations where thin laminations are present and not accounted for, the fluid substitution results are over-predicted and hence small sandstone fractions shows fluid response that is at least twice as much as large sandstone fractions, which might be significantly incorrect.
- Conclusively, this research has shown that conventional wire-line log data can be used as an alternative to core analysis in determining clay heterogeneity pattern in a clastic reservoir environment.

References

Asquith, G. and Krygowski, D., 2004, Basic well-log analysis: The American Association of Petroleum Geologists. Exploration series 16.

Avseth, P., and Bachrach, R., 2005, Seismic properties of unconsolidated sands: Tangential stiffness, Vp/Vs ratios and diagenesis: 75th Annual Meeting, SEG, Expanded Abstracts, p. 1473-1476.

Avseth P., Mukerji, T., and Marvko, G., 2005, Quantitative Seismic Interpretation - Applying Rock Physics Tools to Reduce Interpretation Risk: Cambridge University Press.

Batzle, M. and Wang, Z., 1992, Seismic properties of pore fluids: Geophysics, **57**, p. 1396-1408.

Castagna, J. P., Batzle, M. L. and Eastwood, R.L., 1985, Relationships between compressional-wave and shear-wave velocities in clastic silicate rocks: Geophysics, **50**, p. 571-581.

Castagna, J.P. and Swan, J., 1997, Principles of AVO cross-plotting, The Leading Edge **12**, p. 337–342.

Comisky, J. T., 2002, Petrophysical analysis and geoplogic model for the Bullwinkle J sands with implications for Time-Lapse reservoir monitoring, Green Canyon Block 65, Offshore Louisiana, Geophysics, The Pennsylvania State University.

Darling, T. 2005, Well logging and Formation evaluation: Elsevier Publishers.

Dvorkin, J., and Gutierrez, M., 2001, Textural sorting effect on elastic velocities: 71st Annual Meeting, SEG, Expanded Abstracts.

Dvorkin, J. and Gutierrez, M.A., 2002, Grain Sorting, Porosity and Elasticity: Petrophysics, 43, no.3, p. 185-196.

Dvorkin, J. and Nur, A., 1996, Elasticity of high-porosity sandstone: Theory for two North Sea data sets: Geophysics, **61**, p. 1363-1370.

Flemings, P.B., Comisky, J., Liu, X., and Lupa, J.A., 2001, Stress-controlled porosity in overpressured sands at Bullwinkle (GC65): Deepwater GoM. Offshore Technology Conference, April 30-May 3, 2001

Gardner, G., Gardner, L., and Gregory, A., 1974 Formation velocity and density – the diagnostic basis for stratigraphic traps: Geophysics, **39**, p. 770-780.

Gassmann, F., 1951, Uber die elastizitat poroser medien: Vier. der Naturforsch. Gesellschaft, **96**, p. 1-23.

Greenberg, M.L. and Castagna, J.P., 1992, Shear-wave velocity estimation in porous rock: Theoretical formulation, preliminary verification and applications: Geophysics Prospecting. **40**, p. 195-209.

Han, D., 1986, Effects of porosity and clay content on acoustic properties of sandstones and unconsolidated sediments: Ph. D. dissertation, Stanford University.

Han, D. H., Nur, A., and Morgan, D., 1986, Effects of porosity and clay content on wave velocities in sandstones: Geophysics, **51**, p. 2093-2 107.

Han, D., 2003, Velocities and porosity of deepwater reservoir sands: Expanded abstract, Fluid/DHI Annual Meeting.

Hashin, Z. and Shtrikman, S., 1963, A variational approach to the elastic behavior of multiphase materials: J. Mech. Phys. Solids, **11**, p. 127-140.

Johnstad, S. E., Dvorkin, J., 1999, Velocity-porosity trends in well log data, SEG Expanded abstracts.

Lalande, S., 2002, Characterization of a Thin-Bedded Reservoir in the Gulf of Mexico: An Integrated Approach," M.S. thesis, Geophysics, Texas A&M University.

Marion, D., Nur, A., Yin, H., and Han, D., 1992, Compressional velocity and porosity in sand-clay mixtures: Geophysics, **57**, p. 554-563.

Marvko, G., Mukerji, T., and Dvorkin, J., 2009, The Rock Physics Handbook – Tools for Seismic Analysis in Porous Media (2nd edition): Cambridge University Press.

McCarthy, P., Brand, J., Paradiso, B., Ezekwe, J., Wiltgen, N., Bridge, A., Willingham, R., and Bogaads, M., 2006, Using Geostatistical Inversion of Seismic and Borehole Data to Generate Reservoir Models for Flow Simulations of Magnolia Field, Deepwater Gulf of Mexico: 6th International Conference & Exposition on Petroleum Geophysics "Kolkata 2006"

Mode, A. W. and Adepehin, E. J., 2012, Petrophysical Effects of Clay Heterogeneity on Reservoirs' Properties: Case Study of Brown Field, Niger Delta, NAPE mini Conference Nigeria, Expanded Abstracts.

Murphy, W., Reischer, A., and Hsu., K.,1993, Modulus decomposition of compressional and shear velocities in sand bodies: Geophysics, **58**, p. 227-239.

Nasser, M., 2010, Rock physics – Modeling impact of pore fluid, lithology and depth on AVO signatures, SEG, Expanded Abstracts, p. 373–377

Nasser, M., Escobar, I., and Hans-Peder Hansen, 2013, Rock physics evaluation of deepwater reservoirs, West Africa: 84th Annual International Meeting, SEG, Expanded Abstracts, p. 2407-2411

Nasser, M., Mavko, G., and Dvorkin, J., 2012, Rock physics analysis of deepwater sediments; West Africa: GSH Journal, Vol. 2, No. 6, p. 11-14

Nur, A., Mavko, G., Dvorkin, J., and Galmudi, D., 1998, Critical porosity: A key to relating physical properties to porosity in rocks: The Leading Edge, **17**, p. 357-362.

Oyetunji, O. O., 2013, Integrating rock physics and seismic inversion for reservoir characterization in the Gulf of Mexico, M.S. thesis, Geophysics, University of Houston.

Prather, B. E., Booth, J. R., Steffens, G. S. & Craig, P. A., 1998, Classification, lithologic calibration, and stratigraphic succession of seismic facies of intraslope basins, deep-water Gulf of Mexico: American Association of Petroleum Geologists Bulletin, 82, p. 701-728.

Raymer, L. L., Hunt, E. R., and Gardner, J. S., 1980, An improved sonic transit time-to-porosity transform: 21st Ann. Logg. Symp., SPWLA, p. 1-12.

Reuss, A., 1929, Berechnung der Fliessgrenzen von Mischkristallen auf Grund der Plastizitatsbedingung fur Einkristalle: Zeitschrift fiir Angewandte Mathematik und Mechanik, **9**, p. 49-58.

Rob Simm and Mike Bacon, 2014, Seismic Amplitude: An interpreter's handbook: Cambridge University Press

Said, A.A., Abdallah, M. E., and Alaa, E., 2003, Applications of well logs to assess the effects of clay mineral on petrophysical parameters of lower Cretaceous reservoirs, North Sinai, Egypt

Schlumberger, 1972, Log interpretation: Volume I – Principles, New York, Schlumberger Limited, p.31

Serra, O., 1986, Fundamentals of well log interpretation: Vol. 2, Developments in Petroleum science. El-Sevier. Publishers Co., Amsterdam

Sheriff, R. E., 2006, Encyclopedic Dictionary of Applied Geophysics (4th Edition): Society of Exploration Geophysicists Tulsa, Oklahoma, USA.

Smith, T.M., Sondergeld, C.H. and Rai, C.S., 2003, Gassmann fluid substitutions: A Tutorial: Geophysics, **68**, p. 430-440.

Thomas, E. C., Steiber, S. J., 1975, The distribution of shale in sandstone and its effect upon porosity, SPWLA, 16th Annual Logging Symposium, p. 1-17.

Truman, R.B., Howard, W.E., and Luffel, D.L., 1989, Shale porosity - its impact on well log modeling and interpretation: SPWLA Symposium, 30th, Transactions, p. Q1- Q15.

Vernik, L., 1998, Acoustic velocity and porosity systematics in siliciclastics: The Log Analyst, **39**, p. 27-35.

Voigt, W., 1928, Lehrbuch der Kristallphysik: Teubner, Eeipzig, Germany

Voigt, W., 1952, The elastic behavior of crystalline aggregate: Proc. Physical Soc., London, **A65**, p. 349-354.

Wang, Z., 2001, Fundamentals of seismic rock physics: Geophysics, **66**, p. 398–412.

Wang, Z., Wang, H., and Cates, M. E., 2001, Effective elastic properties of clays: Geophysics, **66**, p. 428–440.

Weimer, P. et al., 1998, Evaluating the Petroleum Systems of the Northern Deep Gulf of Mexico through Integrated Basin Analysis: An Overview: AAPG Bulletin, 1998, 82, No 5B, p. 865-877.

Weissenburger, K. S., and Boras, T., 2004, Fluid properties, phase and compartmentalization: Magnolia Field case study, Deepwater Gulf of Mexico, USA: Geological Society, London, Special Publications 2004, V. 237, p. 231-255

Wenworth, C. K., 1922, A scale of grade class terms for clastic sediments. J. Geol., **30**, p. 377-392

Wood, A. W., 1955, A Textbook of Sound: The MacMillan Co.

Worthington P.F., 2003, Effect of clay content upon some physical properties of sandstone reservoirs: International Association of Sedimentologists. Special Publication, No 34, p. 191–211.

Wyllie, M. R. J., Gregory, A. R. and Gardner, L. W., 1956, Elastic wave velocities in heterogeneous and porous media: Geophysics, **21**, p. 41-70